Path-integral representation for quantum spin models: Application to the quantum cavity method and Monte Carlo simulations

Florent Krzakala
Laboratoire PCT, CNRS et ESPCI ParisTech, Unité Mixte de Recherche (UMR 7083 Gulliver), 10 rue Vauquelin, 75231 Paris, France

Alberto Rosso
LPTMS, CNRS, Université Paris-Sud, UMR8626, Bât. 100, 91405 Orsay Cedex, France

Guilhem Semerjian and Francesco Zamponi
LPTENS, CNRS et ENS, Associée à l'UPMC Univ Paris 06, Unité Mixte de Recherche (UMR 8549), 24 Rue Lhomond, 75231 Paris Cedex 05, France
(Received 16 July 2008; published 30 October 2008)

The cavity method is a well-established technique for solving classical spin models on sparse random graphs (mean-field models with finite connectivity). Laumann *et al.* [Phys. Rev. B **78**, 134424 (2008)] proposed recently an extension of this method to quantum spin-1/2 models in a transverse field, using a discretized Suzuki-Trotter imaginary-time formalism. Here we show how to take analytically the continuous imaginary-time limit. Our main technical contribution is an explicit procedure to generate the spin trajectories in a path-integral representation of the imaginary-time dynamics. As a side result we also show how this procedure can be used in simple heat bath Monte Carlo simulations of generic quantum spin models. The replica symmetric continuous-time quantum cavity method is formulated for a wide class of models and applied as a simple example on the Bethe lattice ferromagnet in a transverse field. The results of the methods are confronted with various approximation schemes in this particular case. On this system we performed quantum Monte Carlo simulations that confirm the exactness of the cavity method in the thermodynamic limit.

DOI: 10.1103/PhysRevB.78.134428 PACS number(s): 05.30.−d, 03.67.Ac, 64.70.Tg, 75.10.Jm

I. INTRODUCTION

Mean-field approximations are often useful first steps to unveil the physical content of realistic models. This is all the more true when exact solutions are probably impossible to obtain in the finite-dimensional setting, in particular when quenched disorder and/or quantum effects have to be taken into account, as for instance in the case of Anderson localization.[1] Another example is dynamical mean-field theory,[2] which has been a very fertile approach to the problem of strongly correlated fermions. It can be sometimes preferable to study mean-field theories not by making an approximation to a finite-dimensional model but rather by formulating a model which is mean field by nature, as this allows in particular to state the results in a mathematically clearer way. The simplest of such examples is the Curie-Weiss model of ferromagnetism, in which N classical Ising spins all interact attractively with each other, with a coupling-constant scaling inversely with the size of the system to ensure a well-defined thermodynamic limit. The equivalent for quenched disordered systems is the Sherrington-Kirkpatrick model[3] of a spin glass, where again all spins interact weakly with each other, yet with coupling constants of random signs.

The mean-field character of the above mentioned models arises from their infinite connectivity (in the thermodynamic limit). There exists however another class of models, which are still mean field yet keep a finite connectivity, each of the degrees of freedom they possess interacting only with a finite (with respect to N) number of neighbors. For ferromagnetic models they can be obtained by the Cayley tree construction, where one draws an infinite regular tree and studies the magnetization of the root site.[4] Cayley tree models have however pathological surface effects, and the theory of finitely connected mean-field frustrated systems is better defined on random graphs,[5,6] of fixed or fluctuating connectivity. Classical models of spins on such random structures have been the subject of extensive study in the last decade. These works were motivated on the one hand by their somehow more physically realistic features, namely, the finite connectivity, and also because of their strong relationship with issues originating from computer science, namely, the understanding of phase transitions in random constraint satisfaction problems.[7–9] Finite-connectivity models are technically much more involved than their fully connected counterparts. The replica method[10] that has been first developed to solve the Sherrington-Kirkpatrick model[3] becomes less practical in this setting,[11] and the alternative cavity method turned out to be more useful.[6]

The interplay between quenched disorder and quantum fluctuations can lead to a very rich phenomenology, and in particular the properties of the glass phase found at low temperatures in classical models can be qualitatively modified when a transverse field acts on the system.[12] More generally the issue of the nature of the quantum phase transitions at zero temperature[13] in presence of disorder is a very rich one. In the context of mean-field theory this point has been mainly studied in fully connected models,[14–20] with a few exceptions that appeared in the last year.[21–24] In a very interesting contribution Laumann *et al.*,[21] made a first step in

extending the cavity method to quantum spin models in a transverse field, and in this paper we shall develop further this idea by solving a discretization problem which plagued their proposal. Let us also mention here the work of Knysh and Smelyanskiy,[23] who developed a similar approach in the framework of the so-called static approximation.[14,16,18] The motivation for this line of work is twofold. On the one hand one can expect an even richer physical behavior of finitely connected quantum models with respect to the fully connected ones. The possible fluctuations in the local geometry and some notion of distance which was absent in fully connected models open the way to a more complex phenomenology. On the other hand one can aim at a better understanding of some issues of quantum computing and in particular on the use of quantum annealing (or adiabatic algorithm)[25–27] to solve random constraint satisfaction problems. These quantum algorithms do indeed rely on the application of a transverse field on spin models that have been extensively studied at the classical level with the cavity method. Computing the location and nature of the phase transitions[28] encountered along the annealing path (as the transverse field is progressively turned off) might give some information on the behavior of these quantum algorithms themselves.

The remaining of the paper is organized as follows. In Sec. II we recall the Suzuki-Trotter approach to spin-1/2 models in a transverse field and develop our main technical contribution in Sec. II B, where we show how to actually build the spin trajectories of the path-integral representation of the imaginary-time evolution operator. Section III is then devoted to the study of a very simple example of finitely connected quantum model, namely, the Bethe lattice ferromagnet. We first explain the continuous-time quantum cavity treatment of this model before presenting the results of the method and confronting them with some approximate approaches. In Sec. IV we present numerical results of Monte Carlo simulations we performed for this model and show how the computations of Sec. II B can be turned in a simple and versatile quantum Monte Carlo method. The generic formalism of the quantum cavity method is developed in Sec. V; we hope this order of presentation and the inclusion of a fully worked-out example before the general case will ease the reading of this work. We finally draw our conclusions and put forward perspectives for future work in Sec. VI. Some technical details are deferred to a series of appendixes.

II. PATH-INTEGRAL REPRESENTATION FOR SPIN-1/2 MODELS

A. Spin models in a transverse field: Suzuki-Trotter formalism

Let us consider the Hilbert space spanned by the orthonormal basis of 2^N kets $|\underline{\sigma}\rangle$, where $\underline{\sigma}=(\sigma_1,\ldots,\sigma_N)$ denotes a configuration of N Ising spins, $\sigma_i=\pm 1$. This space can be viewed as the tensorial product of N spin 1/2, with operators σ_i^z and σ_i^x, whose action on the base vectors is defined by

$$\sigma_i^z|\underline{\sigma}\rangle = \sigma_i|\underline{\sigma}\rangle,$$

$$\sigma_i^x|\underline{\sigma}\rangle = |\sigma_1,\ldots,\sigma_{i-1},-\sigma_i,\sigma_{i+1},\ldots,\sigma_N\rangle. \tag{1}$$

From a classical energy function of N Ising spins, $E(\sigma_1,\ldots,\sigma_N)$, one can construct an operator $\hat{E}=E(\sigma_1^z,\ldots,\sigma_N^z)$, diagonal in the $\{|\underline{\sigma}\rangle\}$ basis. The Hamiltonian operators investigated in this paper are obtained from such a classical energy by the addition of a transverse field,

$$\hat{H}=\hat{E}-B\sum_{i=1}^{N}\sigma_i^x, \quad \text{with } B\geq 0. \tag{2}$$

Our goal is then to compute the quantum statistical-mechanics properties at inverse temperature β, i.e., the partition function Z and the average of observables (operators) $\hat{O}$, defined by

$$Z=\mathrm{Tr}(e^{-\beta\hat{H}}), \quad \langle\hat{O}\rangle=\frac{\mathrm{Tr}(\hat{O}e^{-\beta\hat{H}})}{\mathrm{Tr}(e^{-\beta\hat{H}})}. \tag{3}$$

A well-known way of tackling such problems is to transform them into an extended Ising model by using the Suzuki-Trotter formula,[29] as summarized in the following lines:

$$\begin{aligned}
Z &= \mathrm{Tr}\left\{\left[\exp\left(-\frac{\beta}{N_s}\hat{E}+\frac{\beta}{N_s}B\sum_{i=1}^{N}\sigma_i^x\right)\right]^{N_s}\right\} \\
&= \lim_{N_s\to\infty}\mathrm{Tr}\left\{\left[\exp\left(-\frac{\beta}{N_s}\hat{E}\right)\exp\left(\frac{\beta}{N_s}B\sum_{i=1}^{N}\sigma_i^x\right)\right]^{N_s}\right\} \\
&= \lim_{N_s\to\infty}\sum_{\underline{\sigma}^1,\ldots,\underline{\sigma}^{N_s}}\prod_{\alpha=1}^{N_s}\langle\underline{\sigma}^{\alpha}|\exp\left(-\frac{\beta}{N_s}\hat{E}\right)\exp\left(\frac{\beta}{N_s}B\sum_{i=1}^{N}\sigma_i^x\right)|\underline{\sigma}^{\alpha+1}\rangle \\
&= \lim_{N_s\to\infty}\sum_{\underline{\sigma}^1,\ldots,\underline{\sigma}^{N_s}}\prod_{\alpha=1}^{N_s}\exp\left(-\frac{\beta}{N_s}E(\underline{\sigma}^{\alpha})\right)\prod_{i,\alpha}\langle\sigma_i^{\alpha}|\exp\left(\frac{\beta}{N_s}B\sigma^x\right)|\sigma_i^{\alpha+1}\rangle.
\end{aligned} \tag{4}$$

In the two last lines $\underline{\sigma}^{N_s+1}=\underline{\sigma}^1$. For a finite value of the number of Suzuki-Trotter "slices" N_s, the problem has thus become one of $N\times N_s$ Ising spins, each of the σ_i being promoted to a ring $(\sigma_i^1,\ldots,\sigma_i^{N_s})$ with nearest-neighbor ferromagnetic interactions along the "discrete imaginary-time" α axis (with periodic boundary conditions). The original interaction E acts identically and independently on each of the configurations $\underline{\sigma}^\alpha$. For notational convenience we shall use bold symbols for quantities that depend on the slice α, for instance, $\boldsymbol{\sigma}_i=(\sigma_i^1,\ldots,\sigma_i^{N_s})$ is the configuration of the ring of Ising spins at site i and $\underline{\boldsymbol{\sigma}}=(\underline{\sigma}^1,\ldots,\underline{\sigma}^{N_s})$ is the full configuration of the $N\times N_s$ spins. We can thus introduce a probability measure on the $N\times N_s$ Ising spins,

$$\mu(\underline{\boldsymbol{\sigma}})=\frac{1}{Z_{N_s}}e^{-\beta\tilde{E}(\underline{\boldsymbol{\sigma}})}\prod_{i=1}^{N}w(\boldsymbol{\sigma}_i),$$

$$Z_{N_s}=\sum_{\underline{\boldsymbol{\sigma}}}e^{-\beta\tilde{E}(\underline{\boldsymbol{\sigma}})}\prod_{i=1}^{N}w(\boldsymbol{\sigma}_i), \tag{5}$$

such that the normalization constant Z_{N_s} reduces to the partition function Z in the $N_s\to\infty$ limit (in the following we shall sometimes keep implicit the dependence on N_s). To write in a compact way this last equation we have defined,

$$\tilde{E}(\underline{\boldsymbol{\sigma}})=\frac{1}{N_s}\sum_{\alpha=1}^{N_s}E(\underline{\sigma}^\alpha), \tag{6}$$

the average of independent copies of the classical energy on the various slices and,

$$\begin{aligned}w(\boldsymbol{\sigma})&=\prod_{\alpha=1}^{N_s}\langle\sigma^\alpha|e^{(\beta/N_s)B\sigma^x}|\sigma^{\alpha+1}\rangle\\&=\prod_{\alpha=1}^{N_s}\left[\cosh\left(\frac{\beta B}{N_s}\right)\delta_{\sigma^\alpha,\sigma^{\alpha+1}}+\sinh\left(\frac{\beta B}{N_s}\right)\delta_{\sigma^\alpha,-\sigma^{\alpha+1}}\right],\end{aligned} \tag{7}$$

the ferromagnetic interaction along the imaginary-time axis induced by the transverse field (we use $\sigma^{N_s+1}=\sigma^1$). One can easily show that the average value of observables can be obtained in this formalism as

$$\langle\hat{O}\rangle=\sum_{\underline{\boldsymbol{\sigma}}}\mu(\underline{\boldsymbol{\sigma}})\frac{\langle\underline{\sigma}^\alpha|\hat{O}e^{(-\beta/N_s)\hat{H}}|\underline{\sigma}^{\alpha+1}\rangle}{\langle\underline{\sigma}^\alpha|e^{(-\beta/N_s)\hat{H}}|\underline{\sigma}^{\alpha+1}\rangle}, \tag{8}$$

where the slice number α is here arbitrary, thanks to the cyclic invariance around the discrete imaginary-time axis. This can be simplified further for observables $\hat{O}$ diagonal in the $\{|\underline{\sigma}\rangle\}$ basis, i.e., that can be written as $O(\sigma_1^z,\ldots,\sigma_N^z)$,

$$\langle\hat{O}\rangle=\sum_{\underline{\boldsymbol{\sigma}}}\mu(\underline{\boldsymbol{\sigma}})O(\underline{\sigma}^\alpha)=\sum_{\underline{\boldsymbol{\sigma}}}\mu(\underline{\boldsymbol{\sigma}})\frac{1}{N_s}\sum_{\alpha=1}^{N_s}O(\underline{\sigma}^\alpha). \tag{9}$$

A nondiagonal observable we shall study in the following is the transverse magnetization $\langle\sigma_i^x\rangle$ (written here for an arbitrary site i), which can be computed as

$$\begin{aligned}\langle\sigma_i^x\rangle&=\sum_{\underline{\boldsymbol{\sigma}}}\mu(\underline{\boldsymbol{\sigma}})\frac{1}{N_s}\sum_{\alpha=1}^{N_s}\frac{\langle\sigma_i^\alpha|\sigma^x e^{(\beta/N_s)B\sigma^x}|\sigma_i^{\alpha+1}\rangle}{\langle\sigma_i^\alpha|e^{(\beta/N_s)B\sigma^x}|\sigma_i^{\alpha+1}\rangle}\\&=\sum_{\underline{\boldsymbol{\sigma}}}\mu(\underline{\boldsymbol{\sigma}})\frac{1}{N_s}\sum_{\alpha=1}^{N_s}\left[\tanh\left(\frac{\beta B}{N_s}\right)\right]^{\sigma_i^\alpha\sigma_i^{\alpha+1}}.\end{aligned} \tag{10}$$

B. Continuous imaginary-time limit

To recover the truly quantum properties of the model one has to perform the limit $N_s\to\infty$. The basic degrees of freedom $\boldsymbol{\sigma}_i$ which were the configurations of a ring of Ising spins $(\sigma_i^1,\ldots,\sigma_i^{N_s})$ then become piecewise constant functions $\sigma_i(t)\in\{-1,1\}$ of an imaginary-time parameter t, the discrete coordinate $\alpha\in[1,N_s]$ being mapped to $t\in[0,\beta]$ with the correspondence $t=\beta\alpha/N_s$. In this limit the sum over $\boldsymbol{\sigma}$ in expression (5) of the partition function is naturally interpreted as a path integral. The discreteness of the spin degrees of freedom actually makes such a path-integral representation[30] easier to formulate than Feynman path integrals for continuous coordinates[31] and can be given a rigorous mathematical content.[32–35] Note that these continuous-time trajectories can be easily represented in the memory of a computer, as the trajectory of site i is fully specified by $\sigma_i(t=0)$ and the times at which the spin flips. Actually numerous continuous-time quantum Monte Carlo algorithms do exist (see, for instance, Refs. 36–39).

The rest of the paper will crucially rely on the procedure developed in Secs. II B 2 and II B 3. Though it will also be useful for analytical purposes, it is more intuitively motivated by the following simulational consideration. Maybe the simplest way to ensure the detailed balance condition in a Monte Carlo simulation which aims at sampling an arbitrary measure $\mu(\underline{\sigma})$ is to perform transitions from the current configuration $\underline{\sigma}$ to a configuration obtained by replacing the value of a randomly chosen degree of freedom σ_i by a random value drawn from the measure conditioned on all other degrees of freedom. This procedure is known in classical simulations as the heat bath or Glauber algorithm. Its equivalent in quantum simulations consists in drawing a new configuration of the ring $\boldsymbol{\sigma}_i$ or of the trajectory $\sigma_i(t)$ in the continuous imaginary time, according to the equilibrium measure induced by the spin trajectories of all other sites. A moment of thought reveals that this boils down to study the evolution of a single spin 1/2 in the presence of a constant transverse field and a piecewise constant longitudinal field, the latter being the effective field induced by the rest of the system on $\boldsymbol{\sigma}_i$. This is precisely the issue we shall tackle in Secs. II B 2 and II B 3 after having recalled in Sec. II B 1 the well-established path-integral representation of a spin 1/2.

1. Path-integral representation of a single spin in constant fields

Let us define the propagator for the evolution during an interval of imaginary time λ of a spin in constant transverse and longitudinal fields (B and h, respectively),

$$W(\sigma\to\sigma',h,\lambda)=\langle\sigma|e^{\lambda(h\sigma^z+B\sigma^x)}|\sigma'\rangle. \tag{11}$$

The diagonalization of the order 2 matrix $h\sigma^z+B\sigma^x$ easily leads to

$$W(\sigma \to \sigma', h, \lambda) = \begin{cases} \cosh(\lambda\sqrt{B^2+h^2}) + \sigma \dfrac{h}{\sqrt{B^2+h^2}} \sinh(\lambda\sqrt{B^2+h^2}) & \text{if } \sigma = \sigma' \\ \dfrac{B}{\sqrt{B^2+h^2}} \sinh(\lambda\sqrt{B^2+h^2}) & \text{if } \sigma = -\sigma'. \end{cases} \tag{12}$$

The path-integral representation of this propagator reads[30,38]

$$W(\sigma \to \sigma, h, \lambda) = \sum_{n=0}^{\infty} B^{2n} \int_0^\lambda dt_1 \int_{t_1}^\lambda dt_2 \cdots \int_{t_{2n-1}}^\lambda dt_{2n} \exp[\sigma h(2t_1 - 2t_2 + \cdots - 2t_{2n} + \lambda)], \tag{13}$$

$$W(\sigma \to -\sigma, h, \lambda) = \sum_{n=0}^{\infty} B^{2n+1} \int_0^\lambda dt_1 \int_{t_1}^\lambda dt_2 \cdots \int_{t_{2n}}^\lambda dt_{2n+1} \exp[\sigma h(2t_1 - 2t_2 + \cdots + 2t_{2n+1} - \lambda)]. \tag{14}$$

Each term of these expressions corresponds to a spin trajectory that changes value at times $t_1 < t_2 < \cdots$; it is weighted by a factor B raised to the number of such discontinuities and by $\exp[h\int_0^\lambda \sigma(t)]$. A spin trajectory with identical (opposite) initial and final values has to jump an even (odd) number of times. There are two ways to convince oneself of the correctness of this result. Applying the Suzuki-Trotter formalism to this single spin problem leads to such a weight in the $N_s \to \infty$ limit.[40] Alternatively one can notice that Eqs. (13) and (14) coincide with Eq. (12) at $\lambda = 0$ and that they obey the same set of first-order linear differential equations,

$$\frac{\partial}{\partial \lambda} W(\sigma \to \sigma', h, \lambda) = \sigma' h W(\sigma \to \sigma', h, \lambda) + B W(\sigma \to -\sigma', h, \lambda), \tag{15}$$

which implies that they coincide for all values of λ.

2. Generating trajectories for a constant longitudinal field

The above expressions (13) and (14) can be interpreted as the normalizing constants of probability measures on the set of piecewise constant functions from $t \in [0, \lambda]$ to $\{-1, +1\}$, conditioned on their initial $[\sigma(t=0)]$ and final $[\sigma(t=\lambda)]$ values. More explicitly, for instance, for $\sigma(t=0) = \sigma(t=\lambda) = \sigma$, the probability of a trajectory with $2n$ flips at times in the infinitesimal intervals $[t_j, t_j + dt_j]$, with $t_1 < \cdots < t_{2n}$, is defined to be

$$\frac{1}{W(\sigma \to \sigma, h, \lambda)} B^{2n} e^{\sigma h(2t_1 - 2t_2 + \cdots - 2t_{2n} + \lambda)} dt_1 \cdots dt_{2n}. \tag{16}$$

Our goal is now to construct a procedure for actually sampling from these probability measures, which is constructing spin trajectories according to these weights. We shall do this by exploiting the following two identities:

$$W(\sigma \to \sigma, h, \lambda) = e^{\sigma h \lambda} + B \int_0^\lambda du e^{\sigma h u} W(-\sigma \to \sigma, h, \lambda - u), \tag{17}$$

$$W(\sigma \to -\sigma, h, \lambda) = B \int_0^\lambda du e^{\sigma h u} W(-\sigma \to -\sigma, h, \lambda - u). \tag{18}$$

The path-integral interpretation of these relations, more easily conveyed by the drawing of Fig. 1, is as follows. For the first one, it means that a spin trajectory starting and ending at the same value $\sigma(0) = \sigma(\lambda) = \sigma$ is either constant on the whole time interval or made of a constant part up to time u, followed by a jump to $-\sigma$ and a second part of the trajectory representative of $W(-\sigma \to \sigma, h, \lambda - u)$. Similarly the second one expresses the necessity for a trajectory from σ to $-\sigma$ to have at least one discontinuity at a given time u, followed by a trajectory accounting for $W(-\sigma \to -\sigma, h, \lambda - u)$. These equalities can be proven either from the path-integral representation of Eqs. (13) and (14) or from the explicit expressions of W given in Eq. (12). As a consequence of Eqs. (17) and (18) one obtains the following recursive procedure to draw a spin trajectory for a constant longitudinal field on a time interval of length λ, constrained to $\sigma(0) = \sigma$, $\sigma(\lambda) = \sigma'$:

(i) If $\sigma = -\sigma'$, draw a random variable $u \in [0, \lambda]$ with density proportional to $e^{\sigma h u} W(-\sigma \to -\sigma, h, \lambda - u)$ [see below in Eq. (19) for some details on how to perform this step], set $\sigma(t) = \sigma$ up to time u, and call the same procedure to generate a trajectory from $-\sigma$ to $-\sigma$ on the remaining interval of length $\lambda - u$.

(ii) If $\sigma = \sigma'$, with probability $e^{\sigma h \lambda} / W(\sigma \to \sigma, h, \lambda)$, set $\sigma(t) = \sigma$ on the whole time interval and exit the procedure; otherwise, (a) draw a random variable $u \in [0, \lambda]$ with density proportional to $e^{\sigma h u} W(-\sigma \to \sigma, h, \lambda - u)$, (b) set $\sigma(t) = \sigma$ up to time u, and (c) call the same procedure to generate a trajectory from $-\sigma$ to σ on the remaining interval of length $\lambda - u$.

In order to draw $u \in [0, \lambda]$ with a density proportional to $e^{\sigma h u} W(-\sigma \to -\sigma, h, \lambda - u)$, we compute its cumulative distribution,

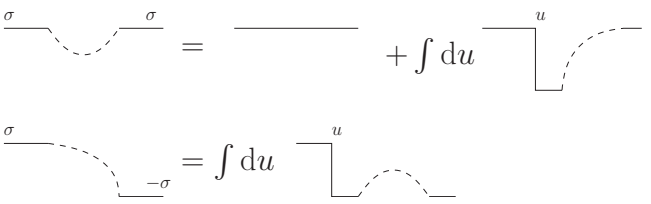

FIG. 1. A pictorial representation of Eqs. (17) and (18).

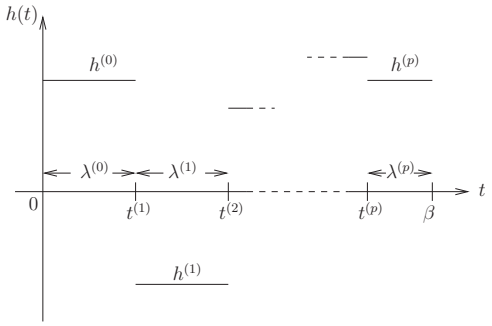

FIG. 2. Definition of the effective-field trajectory.

$$G(u) = \frac{\int_0^u dt e^{\sigma h t} W(-\sigma \to -\sigma, h, \lambda - t)}{\int_0^\lambda dt e^{\sigma h t} W(-\sigma \to -\sigma, h, \lambda - t)}$$

$$= 1 - e^{\sigma h u} \frac{\sinh[(\lambda - u)\sqrt{B^2 + h^2}]}{\sinh(\lambda \sqrt{B^2 + h^2})}. \quad (19)$$

A simple way to draw u amounts to draw G uniformly at random on $[0,1]$ and to invert the above expression to obtain $u(G)$. One can proceed similarly for the generation with the density proportional to $e^{\sigma h u} W(-\sigma \to \sigma, h, \lambda - u)$, which involves another cumulative distribution G.

3. Generating trajectories for a piecewise constant longitudinal field

In Sec. II B 2 we considered the particular case of a constant longitudinal field h. Let us now address the general case of a piecewise constant $\boldsymbol{h} = h(t)$ on the interval of imaginary time $[0, \beta]$, with the following definitions illustrated in Fig. 2: we shall call p the number of times it changes value between $t=0$ and $t=\beta$, $0 = t^{(0)} \leq t^{(1)} \leq \cdots \leq t^{(p)} \leq t^{(p+1)} = \beta$ the times of these changes, $\lambda^{(i)} = t^{(i+1)} - t^{(i)}$ the length of these intervals for $i \in [0,p]$, and finally $h^{(i)}$ the values the field takes in each of these intervals. We shall have to compute the partition function of a spin acted on by such a field,

$$\mathcal{Z}(\boldsymbol{h}) = \mathrm{Tr}\left(\prod_{i=0}^{p} e^{\lambda^{(i)}(h^{(i)}\sigma^z + B\sigma^x)} \right), \quad (20)$$

and to generate spin trajectories according to the corresponding weights. The computation of the partition function can be performed by inserting $p+1$ representations of the identity in Eq. (20), corresponding to the spin values at the imaginary times $t^{(i)}$ where $h(t)$ is discontinuous,

$$\mathcal{Z}(\boldsymbol{h}) = \sum_{\sigma_0, \ldots, \sigma_p} \mathcal{Z}(\sigma_0, \ldots, \sigma_p | \boldsymbol{h}),$$

$$\mathcal{Z}(\sigma_0, \ldots, \sigma_p | \boldsymbol{h}) = \prod_{i=0}^{p} W(\sigma_i \to \sigma_{i+1}, h^{(i)}, \lambda^{(i)}), \quad (21)$$

with $\sigma_{p+1} = \sigma_0$. Given the trajectory $\boldsymbol{h}$ this computation is easily performed, necessitating only the multiplication of the p matrices of order 2 defined in Eq. (11). The sampling of the spin trajectory $\sigma(t)$ on the interval $[0, \beta]$ is done as follows. The values $(\sigma_0, \ldots, \sigma_p)$ of the spin at times $(t^{(0)}, \ldots, t^{(p)})$ are generated[41] according to the probability $\mathcal{Z}(\sigma_0, \ldots, \sigma_p | \boldsymbol{h}) / \mathcal{Z}(\boldsymbol{h})$. Then for each interval $i \in [0,p]$ a spin trajectory from σ_i to σ_{i+1} is generated according to the procedure of Sec. II B 2, the longitudinal field being constantly equal to $h^{(i)}$ on this interval of time. Finally the $p+1$ trajectories are concatenated to obtain the full trajectory from $t=0$ to $t=\beta$.

Let us emphasize that the path-integral representation of the imaginary-time evolution is well known in the literature;[30–35] however we could not find in previous works such an explicit sampling procedure for generating the spin trajectories. Actually, as far as we know, all continuous-time quantum Monte Carlo algorithms[36–39] do not proceed in a heat-bath way (i.e., by generating "from scratch" a new spin trajectory conditioned on the local effective field) but rather construct the spin update using the current configuration itself.

III. QUANTUM BETHE LATTICE FERROMAGNET

The remainder of this paper will be devoted to the study of the simplest of the finitely connected models that can be handled by the quantum cavity method, namely, the transverse field quantum spin-1/2 ferromagnet on the Bethe lattice (more precisely on a random regular graph). The physical properties of such a model are very intuitive: at low temperature and transverse field the model is ferromagnetically ordered, with a positive spontaneous longitudinal magnetization. Thermal (increasing T) or quantum (increasing B) fluctuations destroy this order outside a region delimitated by a critical line in the (B,T) plane, which ends up in a quantum critical point at zero temperature.

An even simpler model displaying these features is the (fully connected) quantum Curie-Weiss model, whose solution we recall in Appendix A. Both of them are of a mean-field nature and should share most of their qualitative properties, yet the Bethe lattice model is quantitatively different and technically more involved because of its finite connectivity.

A. Quantum cavity method treatment

The quantum Bethe lattice ferromagnet is defined by the Hamiltonian

$$\hat{H} = -\sum_{i-j} \sigma_i^z \sigma_j^z - B \sum_{i=1}^{N} \sigma_i^x, \quad (22)$$

where the first sum runs over the edges of a random $l+1$-regular graph of N vertices.[42] This means that the graph of interactions is uniformly chosen among all graphs on N vertices for which each vertex has the same number $l+1$ of neighbors. These graphs have the good properties to realize finite-size Bethe lattices: the set of vertices at distance[43] smaller than a given cutoff d from an arbitrarily chosen vertex is, with a probability which goes to one when N diverges with d held fixed, a regular tree of connectivity $l+1$. On the other hand such a graph has no surface, contrarily to the

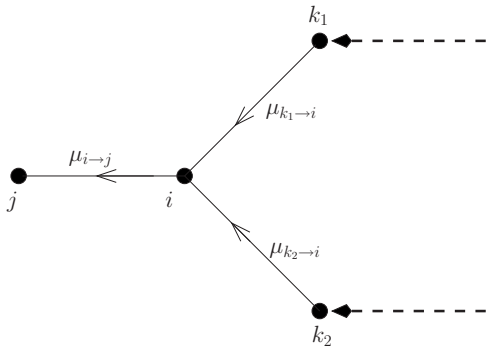

FIG. 3. A pictorial representation of Eq. (23).

usual Cayley tree, and the problem of the boundary conditions for frustrated models (that will be encompassed by the generic treatment of Sec. V) is absent with such a definition.

The hypotheses of the cavity method are more simply explained assuming first that the graph of interactions is actually a finite tree and that the quantum aspects of the problem have been handled by a finite number N_s of Suzuki-Trotter slices. In such a case it is easy to solve the model exactly by taking benefit of the natural recursive structure of a tree: one breaks the graph of interaction into subtrees that are then glued together. Let us explain this with more precise formulas, defining $\mu_{i\to j}(\boldsymbol{\sigma}_i)$ as the probability law of the configuration of the ring $\boldsymbol{\sigma}_i$ when the interaction with its neighbor j has been removed from the graph. If we denote by ∂i the set of vertex neighbors of i, the recurrence equations for these distributions are

$$\mu_{i\to j}(\boldsymbol{\sigma}_i) = \frac{1}{z_{i\to j}} w(\boldsymbol{\sigma}_i) \prod_{k\in\partial i\setminus j} \sum_{\boldsymbol{\sigma}_k} \mu_{k\to i}(\boldsymbol{\sigma}_k) e^{\beta\boldsymbol{\sigma}_i\cdot\boldsymbol{\sigma}_k}, \quad (23)$$

where $z_{i\to j}$ is a normalization constant, and we introduced for two arbitrary imaginary-time dependent quantities $\boldsymbol{a}\cdot\boldsymbol{b} = \sum_{\alpha=1}^{N_s} a^\alpha b^\alpha / N_s$. A graphical representation of this equation is given in Fig. 3 in the case $l=2$. Site i has then two neighbors, k_1 and k_2. The distributions $\mu_{k_{1,2}\to i}$ encode the effect on $k_{1,2}$ of the part of the tree that does not involve i; this is represented by the dashed line in Fig. 3. In absence of site i sites k_1 and k_2 are decoupled (as we assume the graph to be a tree there are no paths between k_1 and k_2 that do not go across i) and hence independent. Therefore the distribution of $\boldsymbol{\sigma}_i$ in absence of site j is given by Eq. (23). A proof of such recursion equations and a discussion of the connections with the Bethe-Peierls approximation and the belief propagation algorithm can be found in Refs. 44 and 45. On a given tree this set of equations (one for each directed edge of the graph) has a unique solution, which is a set of "messages" $\mu_{i\to j}$, that can be efficiently determined by sweeping the edges from the leaves toward the center of the tree. From them all the relevant thermodynamic quantities can be computed. For instance, the probability law of the configuration of the ring $\boldsymbol{\sigma}_i$ in the complete tree is given in terms of the messages sent by its neighbors,

$$\mu(\boldsymbol{\sigma}_i) = \frac{1}{z_i} w(\boldsymbol{\sigma}_i) \prod_{k\in\partial i} \sum_{\boldsymbol{\sigma}_k} \mu_{k\to i}(\boldsymbol{\sigma}_k) e^{\beta\boldsymbol{\sigma}_i\cdot\boldsymbol{\sigma}_k}, \quad (24)$$

with z_i as a normalization constant, while the joint law for two neighboring sites i and j reads

$$\mu(\boldsymbol{\sigma}_i,\boldsymbol{\sigma}_j) = \frac{1}{z_{i-j}} \mu_{i\to j}(\boldsymbol{\sigma}_i)\mu_{j\to i}(\boldsymbol{\sigma}_j) e^{\beta\boldsymbol{\sigma}_i\cdot\boldsymbol{\sigma}_j}. \quad (25)$$

Moreover the free energy per site f can be expressed in terms of the normalization constants of these laws,

$$-\beta f = \frac{1}{N}\ln Z = \frac{1}{N}\sum_{i=1}^{N} \ln z_i - \frac{1}{N}\sum_{i-j} \ln z_{i-j}, \quad (26)$$

where the second sum runs over the (undirected) edges of the tree.

The above derivation was exact because we assumed the graph of interactions to be a tree. The scope of the cavity method is to extend these results to random graphs which are only locally treelike in the precise sense explained above. In its simplest version, called replica symmetric for historical reasons, one assumes the existence of a single pure state in the configuration space of the random graph model. This implies a decay of correlations at large distance in the graph; hence the effect of the long loops neglected in the tree derivation amounts to create a self-consistent boundary condition which traduces the absence of a surface in the random graph. As in the present model all sites have the same neighborhood (there is no fluctuation neither in the connectivity nor in the intensity of the interaction couplings), one has to look for a solution of Eq. (23) where the messages $\mu_{i\to j}$ are all equal to a single law, which we shall denote in the following $\eta(\boldsymbol{\sigma})$, which is seen from Eq. (23) to satisfy

$$\eta(\boldsymbol{\sigma}) = \frac{1}{z_l} w(\boldsymbol{\sigma}) \left(\sum_{\boldsymbol{\sigma}'} \eta(\boldsymbol{\sigma}') e^{\beta\boldsymbol{\sigma}\cdot\boldsymbol{\sigma}'} \right)^l. \quad (27)$$

The assumption on the unicity of the pure state can fail for two kinds of reasons. In ferromagnetic models, as the one considered now, there is an ordered phase at low temperature and transverse field in which two pure states coexist because of the up/down symmetry of the model. This is not a serious limitation of the method; in the following it will be kept understood that an infinitesimal longitudinal field is applied to the system in order to select one of the two pure states. In fact, the exactness of the cavity method for classical ferromagnetic models on random graphs has been recently proven rigorously.[46] A much more serious problem, which shall not be discussed in this paper, arises in frustrated models when an exponential number of pure states proliferate at low temperatures; the replica-symmetry-breaking version of the cavity method is then required to solve the problem.

Let us first write the solution of Eq. (27) in the classical situation for $B=0$. In such a case the weight w forces all spins along the ring to take the same value, hence

$$\eta(\boldsymbol{\sigma}) = \frac{1+\tanh(\beta h)}{2} \left(\prod_{\alpha=1}^{N_s} \delta_{\sigma^\alpha,1} \right) + \frac{1-\tanh(\beta h)}{2} \left(\prod_{\alpha=1}^{N_s} \delta_{\sigma^\alpha,-1} \right), \quad (28)$$

where h is solution of

$$h = \frac{l}{\beta}\text{arctanh}[\tanh(\beta)\tanh(\beta h)]. \tag{29}$$

The classical model thus exhibits a continuous paramagnetic to ferromagnetic transition when the inverse temperature β crosses its critical value, $\beta_c = \text{arctanh}(1/l)$.

We now come back to the general B case and rewrite explicitly the cavity method prediction for the free energy per site, which is obtained from Eq. (26) by substituting $\mu_{i\to j} = \eta$,

$$-\beta f = \ln\left\{\sum_{\boldsymbol{\sigma}} w(\boldsymbol{\sigma})\left[\sum_{\boldsymbol{\sigma}'} \eta(\boldsymbol{\sigma}')e^{\beta\boldsymbol{\sigma}\cdot\boldsymbol{\sigma}'}\right]^{l+1}\right\} - \frac{l+1}{2}\ln\left[\sum_{\boldsymbol{\sigma},\boldsymbol{\sigma}'} \eta(\boldsymbol{\sigma})\eta(\boldsymbol{\sigma}')e^{\beta\boldsymbol{\sigma}\cdot\boldsymbol{\sigma}'}\right], \tag{30}$$

and for the probability law on one site and two adjacent sites,

$$\mu(\boldsymbol{\sigma}) = \frac{1}{z_{l+1}} w(\boldsymbol{\sigma})\left(\sum_{\boldsymbol{\sigma}'} \eta(\boldsymbol{\sigma}')e^{\beta\boldsymbol{\sigma}\cdot\boldsymbol{\sigma}'}\right)^{l+1},$$

$$\mu(\boldsymbol{\sigma},\boldsymbol{\sigma}') = \frac{1}{z_{\text{edge}}} \eta(\boldsymbol{\sigma})\eta(\boldsymbol{\sigma}')e^{\beta\boldsymbol{\sigma}\cdot\boldsymbol{\sigma}'}. \tag{31}$$

Note that expression (30) is variational in the sense that its derivative with respect to η vanishes on the solution of Eq. (27).

B. Convenient representation of $\eta(\boldsymbol{\sigma})$

We turn now to the problem of the determination of the probability law $\eta(\boldsymbol{\sigma})$ solution of Eq. (27). As this is a law on the probability of N_s Ising spins, its complete characterization should involve $2^{N_s}-1$ real numbers. Such a direct representation becomes very soon impossible to handle when N_s grows and in particular in the continuous-time limit $N_s \to \infty$. We shall however see that an alternative representation allows us to bypass this difficulty. First we define a probability law $p(\boldsymbol{\sigma}|\boldsymbol{h})$ on the configurations of a ring of spins $\boldsymbol{\sigma}$ by

$$p(\boldsymbol{\sigma}|\boldsymbol{h}) = \frac{1}{\mathcal{Z}(\boldsymbol{h})} w(\boldsymbol{\sigma})e^{\beta\boldsymbol{\sigma}\cdot\boldsymbol{h}}, \quad \mathcal{Z}(\boldsymbol{h}) = \sum_{\boldsymbol{\sigma}} w(\boldsymbol{\sigma})e^{\beta\boldsymbol{\sigma}\cdot\boldsymbol{h}}, \tag{32}$$

where $\mathcal{Z}(\boldsymbol{h})$ ensures the normalization of $p(\boldsymbol{\sigma}|\boldsymbol{h})$. These definitions allow us to rewrite Eq. (27) as

$$\eta(\boldsymbol{\sigma}) = \sum_{\boldsymbol{\sigma}_1,\ldots,\boldsymbol{\sigma}_l} \eta(\boldsymbol{\sigma}_1)\cdots\eta(\boldsymbol{\sigma}_l)p(\boldsymbol{\sigma}|\boldsymbol{\sigma}_1+\cdots+\boldsymbol{\sigma}_l) \times \frac{\mathcal{Z}(\boldsymbol{\sigma}_1+\cdots+\boldsymbol{\sigma}_l)}{z_l}. \tag{33}$$

Suppose now that one has an estimation of $\eta(\boldsymbol{\sigma})$ given by a representative weighted sample of $\mathcal{N}_{\text{traj}}$ elements $\{\boldsymbol{\sigma}_i\}$, which is

$$\eta(\boldsymbol{\sigma}) = \sum_{i=1}^{\mathcal{N}_{\text{traj}}} a_i \delta(\boldsymbol{\sigma}-\boldsymbol{\sigma}_i), \tag{34}$$

such that the weights a_i add up to one. A new estimation of η (i.e., a new set of configurations $\boldsymbol{\sigma}_i'$ and weights a_i') can then be obtained by plugging this estimation in the left-hand side of Eq. (33), which leads to the following procedure. To generate each of the new $\mathcal{N}_{\text{traj}}$ representants of η, one repeats in an independent way the following steps: (i) draw independently l integers $i_1,\ldots,i_l$ in $[1,\mathcal{N}_{\text{traj}}]$ with probability a_i, (ii) set $\boldsymbol{h}=\boldsymbol{\sigma}_{i_1}+\cdots+\boldsymbol{\sigma}_{i_l}$, and (iii) generate a configuration $\boldsymbol{\sigma}_i'$ according to the law $p(\boldsymbol{\sigma}|\boldsymbol{h})$ and set $a_i'=\mathcal{Z}(h)$.

Once the $\mathcal{N}_{\text{traj}}$ new elements have been generated one just has to multiply the weights a_i' by a global normalization factor, and the new estimates can be again plugged in the right-hand side of Eq. (33) to approach its fixed-point solution.

At this point the continuous-time limit $N_s \to \infty$ can be taken without any difficulty of principle: as long as β is finite the spin trajectories have only a finite number of discontinuities and can then be easily encoded with a finite set of reals corresponding to the time they change values. Moreover one can easily show that in this limit drawing a spin trajectory from the law $p(\boldsymbol{\sigma}|\boldsymbol{h})$ corresponds exactly to the procedure we defined in Sec. II B [we show explicitly this correspondence for the normalization $\mathcal{Z}(\boldsymbol{h})$ in Appendix B].

This representation of the probability law $\eta(\boldsymbol{\sigma})$ by a sample of representative elements is a widespread technique in the field of disordered systems.[1,6] We warn however the reader accustomed to the classical cavity method that we did not use it exactly in the usual way as the classical equivalent of $\eta(\boldsymbol{\sigma})$ is a single real number, not a probability law.

Before closing this section let us discuss the computation of the physical observables in the continuous limit, taking as representative examples the longitudinal and transverse magnetizations. These can be obtained by taking the $N_s \to \infty$ limit of formulas (9) and (10), which yields

$$m_z = \lim_{N\to\infty}\frac{1}{N}\sum_{i=1}^{N}\langle\sigma_i^z\rangle = \sum_{\boldsymbol{\sigma}}\mu(\boldsymbol{\sigma})\frac{1}{\beta}\int_0^\beta dt\,\sigma(t),$$

$$m_x = \lim_{N\to\infty}\frac{1}{N}\sum_{i=1}^{N}\langle\sigma_i^x\rangle = \sum_{\boldsymbol{\sigma}}\mu(\boldsymbol{\sigma})\frac{1}{\beta B}j(\boldsymbol{\sigma}), \tag{35}$$

where in the right-hand side $\mu(\boldsymbol{\sigma})$ is to be computed from Eq. (31), the sums over $\boldsymbol{\sigma}$ are understood as sums over continuous-time trajectories, and we have defined $j(\boldsymbol{\sigma})$ as the number of discontinuities of $\sigma(t)$ on the interval $[0,\beta]$.

C. Continuous-time results

We present now numerical results for $l=2$; the behavior is qualitatively the same for any l. We followed the method of resolution presented above using $\mathcal{N}_{\text{traj}}=10^4$ trajectories. For a fixed temperature, we initialized the population at $B=0$; then each trajectory is constant and its value is chosen in such a way that the average magnetization is equal to the classical magnetization that can be obtained from the solution of Eq.

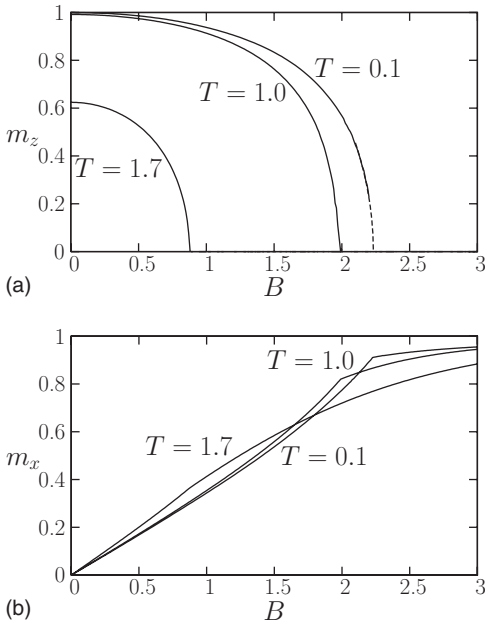

FIG. 4. Longitudinal (m_z, top panel) and transverse (m_x, bottom panel) magnetizations as functions of the transverse field B for $T=1.7,1.0,0.1$. For the lowest temperature we could not obtain reliable data for m_z close to the critical field due to critical fluctuations. The dashed line is a fit to $m_z \sim (B_c - B)^{1/2}$ done in the interval $B \in [2.1,2.2]$ and serves as a guide for the eyes.

(29). In this way we select one of the two possible ferromagnetic states, which we can follow by increasing gradually the transverse field. We increased B with a step $dB=10^{-2}$ and for each step we let the population equilibrate for 10^2 iterations and averaged the observables over 10^3 subsequent steps. We checked that the weights a_i defined in Eq. (34) remain quite uniformly distributed over the population at all investigated temperatures and transverse fields.

In Fig. 4 we plot the magnetizations m_z and m_x as functions of the transverse field B for three different temperatures $T<T_c(B=0)=1/\operatorname{arctanh}(1/2)=1.820\cdots$. At these low temperatures, the system undergoes a continuous phase transition at a critical value $B_c(T)$ of the transverse field. The transition is characterized by the vanishing of m_z and by a jump in the derivative of m_x. Unfortunately obtaining reliable values of m_z close to B_c is a difficult numerical task due to critical fluctuations that cause strong finite-size effects in the size of the population $\mathcal{N}_{\text{traj}}$. Therefore we located the transition by the jump in the derivative of m_x; we fitted m_x by linear laws close to B_c from above and below and determined their intersection.

The resulting phase diagram is reported in Fig. 5. We found that for $T \lesssim 0.3$ the temperature dependence of all observables is very weak and $B_c \sim 2.232$, which is a reliable estimate for the $T \to 0$ limit and is in excellent agreement with the value determined in Ref. 24. The scaling of B_c for $T \to 0$ is compatible with the essential singularity that is found in the Curie-Weiss model [see Appendix A and in particular Eq. (A8)]. The very weak (practically unobservable) temperature dependence of the free energy below $T=0.3$ makes us confident that the entropic term is negligible at these low temperatures and the free energy for $T=0.1$,

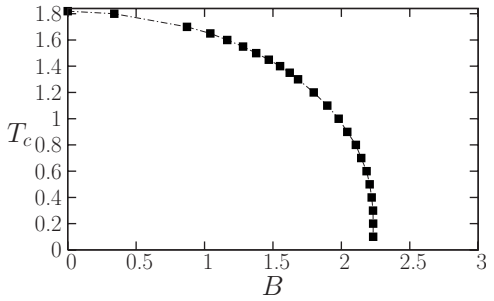

FIG. 5. Phase diagram: the critical temperature T_c as a function of the transverse field B.

plotted in Fig. 6, is representative of the ground-state energy e_{GS}. The latter has a weak singularity (discontinuity of the second derivative) at B_c which is not observable with our numerical precision but is easily observed by a direct computation of $m_x = -\frac{de_{\text{GS}}}{dB}$ (see Fig. 4).

Overall, our results are in very good quantitative agreement with the ones obtained at $T=0$ in Ref. 24 by a matrix product state description, except for the value of the exponent β characterizing the vanishing of the magnetization close to B_c, $m_z \sim (B_c - B)^{\beta}$. Even if we do not have very precise data close to B_c due to finite population-size effects, our data are compatible with the mean-field exponent $\beta=0.5$ at all investigated temperatures, while in Ref. 24 a slightly smaller value of $\beta \sim 0.41$ is reported at $T=0$. We will further comment on this discrepancy in Sec. IV C.

D. Comparison with approximate treatments

In this section we compare the previous results with approximated solutions of Eq. (27). First we consider the finite N_s case, then we consider variational approximations to the solution.

1. Resolution at finite N_s

At finite N_s, the distribution $\eta(\boldsymbol{\sigma})$ can be encoded with $2^{N_s}-1$ real numbers (e.g., the probabilities of each of the 2^{N_s} configuration, with their sum constrained to be 1). Then Eq. (27) can be rewritten as a fixed-point equation for these num-

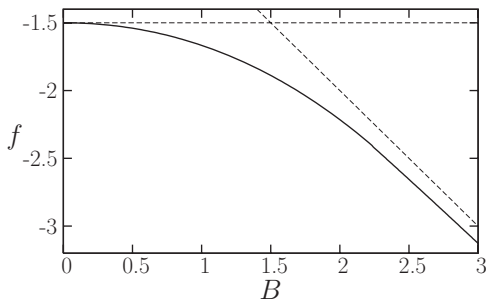

FIG. 6. Free energy as a function of B for $T=0.1$. The curves for $T=0.3,0.2,0.1$ coincide within our numerical precision. Therefore we assume that this curve is representative of the ground-state energy as a function of B. The asymptotic values for $B \to 0$ ($e_{\text{GS}}=3/2$) and for $B \to \infty$ ($e_{\text{GS}}=-B$) are reported as dashed lines. The subleading correction for large B is $\propto B^{-1}$ and is not reported.

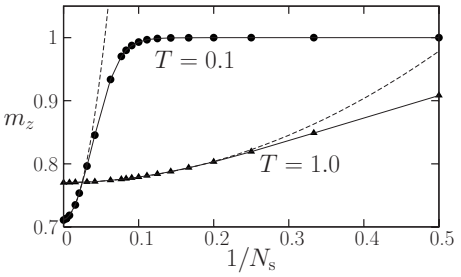

FIG. 7. Longitudinal magnetization m_z as a function of $1/N_s$ for $T=1.0$, $B=1.5$ (triangles) and for $T=0.1$, $B=1.8$ (circles). In both cases the point at $1/N_s=0$ corresponds to the continuous-time result. Full lines are guides for the eyes, dashed lines are fit to quadratic laws, $m_z-m_z(N_s\to\infty)\propto N_s^{-2}$.

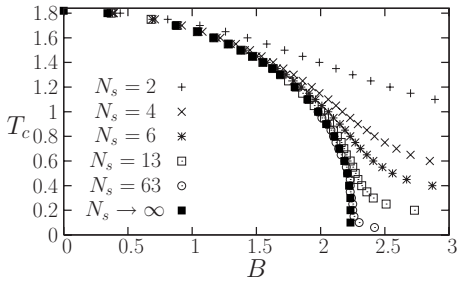

FIG. 8. Phase diagram at finite N_s: the critical temperature T_c as a function of the transverse field B. Note that for a fixed N_s, $T_c(B\to\infty)=T_c(B=0)/N_s$. Filled squares are the result of the continuous-time method, already reported in Fig. 5.

bers, and the solution can be found by simple iteration (below we refer to this procedure as "exact solution" for finite N_s). This method is extremely precise but computationally very heavy, as the time to solve the equation scales exponentially in N_s. We are then limited to $N_s\leq 13$; the computation for the largest $N_s=13$ took two weeks on a standard workstation, while we estimated the one for $N_s=14$ to take at least two months.

Therefore, in order to study the approach to the limit $N_s\to\infty$, we resorted to the population method described in Sec. III B. We represented $\eta(\boldsymbol{\sigma})$ by a population of discrete time trajectories $\boldsymbol{\sigma}=(\sigma^1,\ldots,\sigma^{N_s})$ and solved Eq. (27) by iteration following the procedure detailed in Sec. III B without taking the limit $N_s\to\infty$. Similarly to the continuous-time case, we used $\mathcal{N}_{\text{traj}}=10^5$ and performed 10^2 iterations to achieve convergence, after which data have been collected along 10^3 iterations. The computation time is now polynomial in N_s so we can go to much larger values (at the price of numerical precision due to finite $\mathcal{N}_{\text{traj}}$). Note that the continuous-time computation is much more efficient. In the discrete time case, at low B and large T, the spins σ^α are constant along large time intervals and the information encoded in a discrete trajectory is redundant. On the contrary, at low T and large B the method at finite N_s is obviously incorrect because of the discretization. One could think to adapt N_s in order to find the optimal value for a given T, B; however this is most naturally done in the continuous-time framework where the number of spin flips is the natural variable describing a trajectory. Therefore we think that the finite N_s population method is useful only for the illustrative purposes of this section.

Data reported in this section and in Figs. 7 and 8 have been obtained by exact solution for $N_s\leq 13$ and by the population method for $N_s>13$. We do not report detailed results for the magnetization as a function of B; as expected, the agreement with the continuous-time computation is very good at high temperature and becomes poorer and poorer on lowering the temperature. We focused on two points in the phase diagram: the first at intermediate temperature $T=1.0$ and $B=1.5$; the second at very low temperature $T=0.1$ and $B=1.8$. In Fig. 7 we plot the longitudinal magnetization m_z for different values of N_s. As expected, finite N_s effects are much stronger at low temperature. Note that for large N_s the leading correction is $\propto N_s^{-2}$, as in the Curie-Weiss model (see Appendix A). For $T=1$ deviations from the leading term are very small and $N_s\sim 10$ is enough to get a fair estimate of the true m_z. On the contrary, for $T=0.1$ deviations are very large and $N_s\gtrsim 256$ is needed.

In Fig. 8 we report the critical temperature as a function of B for different values of N_s together with the continuous-time result. Note that in the limit of large transverse field, each of the N_s time slices becomes independent of the others. The model reduces to N_s copies of the classical system ($B=0$) with a ferromagnetic coupling rescaled by $1/N_s$. Then in this limit the critical temperature is given by the classical one divided by N_s, $T_c(N_s,B\to\infty)=1/[N_s\,\text{arctanh}(1/l)]$. Below this temperature the system is always in the ferromagnetic phase, so that the quantum phase transition cannot be studied within this approximation.

For generic spin-1/2 models, the finite N_s approximation might be useful in order to understand the behavior at intermediate temperatures and might also give quantitatively accurate results far from $T=0$. This might be useful in cases where more complicated cavity treatments (such as the so-called *one-step replica-symmetry breaking*) are necessary. Still the continuous-time method appears to us preferable as it remains reliable down to very low temperatures.

2. Static approximation

A different strategy to obtain approximate solutions of these models is to use the variational property of Bethe free energy (30): the free energy of the model is the minimum of the free energy defined by Eq. (30) over the function $\eta(\boldsymbol{\sigma})$ (in the classical case the correctness of this procedure has been proven in Ref. 46). Then one can propose a variational form for $\eta(\boldsymbol{\sigma})$ and minimize the free energy with respect to the free parameters to obtain an upper bound to the true free energy of the problem.

A popular variational form is the so-called *static approximation*, which in our context amounts to the following ansatz for $\eta(\boldsymbol{\sigma})$:

$$\eta(\boldsymbol{\sigma}) = \eta\left[\frac{1}{\beta}\int_0^\beta dt\sigma(t)\right] = \eta\left[\frac{1}{N_s}\sum_{\alpha=1}^{N_s}\sigma_\alpha\right], \qquad (36)$$

i.e., the probability of a trajectory depends only on its average spin value along the imaginary time. This approximation has been widely used in computations based on the replica

method for fully connected models[14–16,18] and has been recently applied to the random k satisfiability in a transverse field.[23] The present derivation based on the cavity method gives back the same results originally derived in Ref. 23 but is simpler because the use of replicas is avoided. Here we discuss only the case of the ferromagnet on a regular graph but the equations can be easily generalized to more complicated cases where fluctuations of the couplings and/or the connectivity are present.[23]

Equivalently we can rewrite the equation above as

$$\eta(\boldsymbol{\sigma}) = \int_{-\infty}^{\infty} dh p(h) \prod_{\alpha=1}^{N_s} \left[\frac{e^{h\sigma_\alpha}}{2\cosh h} \right] = \int_{-1}^{1} dm p(m) \prod_{\alpha=1}^{N_s} \left[\frac{1+m\sigma_\alpha}{2} \right], \tag{37}$$

where with a slight abuse of notation we used p for the distribution of both the effective field h and its associated magnetization $m=\tanh h$. This expression makes evident that the assumption of the static approximation is that the spins in a trajectory are uncorrelated along the imaginary time and subject to a common field extracted from the distribution $p(h)$.

From Eq. (37) it follows that, in the limit $N_s \to \infty$,

$$\sum_{\boldsymbol{\sigma}'} \eta(\boldsymbol{\sigma}') e^{\beta \boldsymbol{\sigma}\cdot\boldsymbol{\sigma}'} = \int_{-1}^{1} dm p(m) \prod_{\alpha=1}^{N_s} \left[\cosh\frac{\beta}{N_s} + m\sigma_\alpha \sinh\frac{\beta}{N_s} \right] \sim \int_{-1}^{1} dm p(m) \prod_{\alpha=1}^{N_s} e^{m\sigma_\alpha \beta/N_s},$$

$$\sum_{\boldsymbol{\sigma},\boldsymbol{\sigma}'} \eta(\boldsymbol{\sigma}) \eta(\boldsymbol{\sigma}') e^{\beta \boldsymbol{\sigma}\cdot\boldsymbol{\sigma}'} = \int_{-1}^{1} dm dm' p(m) p(m') e^{\beta m m'},$$

$$\begin{aligned}
\sum_{\boldsymbol{\sigma}} w(\boldsymbol{\sigma}) \left[\sum_{\boldsymbol{\sigma}'} \eta(\boldsymbol{\sigma}') e^{\beta \boldsymbol{\sigma}\cdot\boldsymbol{\sigma}'} \right]^{l+1} &= \int_{-1}^{1} dm_1 p(m_1) \cdots dm_{l+1} p(m_{l+1}) \sum_{\boldsymbol{\sigma}} w(\boldsymbol{\sigma}) \exp\left[\beta \left(\sum_{p=1}^{l+1} m_p \right) \left(N_s^{-1} \sum_{\alpha=1}^{N_s} \sigma_\alpha \right) \right] \\
&= \int_{-1}^{1} dm_1 p(m_1) \cdots dm_{l+1} p(m_{l+1}) \int_{-1}^{1} dm \exp\left(\beta m \sum_{p=1}^{l+1} m_p \right) \sum_{\boldsymbol{\sigma}} w(\boldsymbol{\sigma}) \delta\left(m - \frac{1}{N_s} \sum_{\alpha=1}^{N_s} \sigma_\alpha \right) \\
&= \int_{-1}^{1} dm_1 p(m_1) \cdots dm_{l+1} p(m_{l+1}) \int_{-1}^{1} dm \exp\left(\beta m \sum_{p=1}^{l+1} m_p \right) w_s(m),
\end{aligned} \tag{38}$$

where in the last line we defined the function

$$w_s(m) = \sum_{\boldsymbol{\sigma}} w(\boldsymbol{\sigma}) \delta\left(m - \frac{1}{N_s} \sum_{\alpha=1}^{N_s} \sigma_\alpha \right). \tag{39}$$

The following explicit expression for $w_s(m)$ can be found in Ref. 23 (where it was called $e^{-\beta u_0(m)}$):

$$w_s(m) = \frac{\beta B}{\sqrt{1-m^2}} I_1(\beta B \sqrt{1-m^2}) + \delta(m-1) + \delta(m+1), \tag{40}$$

with I_1 as the modified Bessel function of the first kind. For completeness we provide a proof of this result in Appendix C. From the equations above one obtains free energy (30) as a functional of $p(m)$, which has then to be minimized. Remarkably, the resulting expression for the free energy is equivalent to the cavity free energy for a classical system whose variables are the continuous $m_i \in [-1,1]$ and whose Gibbs measure is defined by

$$\mu_s(\underline{m}) = \frac{1}{Z_s} e^{-\beta H_s(\underline{m})} = \frac{1}{Z_s} \exp\left(\beta \sum_{i-j} m_i m_j \right) \prod_{i=1}^{N} w_s(m_i), \tag{41}$$

i.e., it is obtained from quantum measure (5) by replacing the quantum operators by their average and the transverse field term by its average as defined in Eq. (39). The analogy with a classical system or a direct differentiation of the free energy with respect to $p(m)$ allows us to write a cavity equation for $p(m)$ which is the analog of Eq. (27),

$$p(m) = \frac{1}{z_l} w_s(m) \left(\int_{-1}^{1} dm' p(m') e^{\beta m m'} \right)^l. \tag{42}$$

Given the structure of $w_s(m)$ it turns out that $p(m)$ can be decomposed as $a_+\delta(m-1)+a_-\delta(m+1)+\tilde{p}(m)$, where $\tilde{p}$ has its support strictly between -1 and 1. We solved Eq. (42) by iteration using a discretized representation of the regular part $\tilde{p}$ and keeping explicitly the weights $a_\pm$. Note that at $B=0$ the first term in Eq. (40) vanishes. Then $a_\pm = [1 \pm \tanh(\beta h)]/2$ where h is the solution of Eq. (29): the

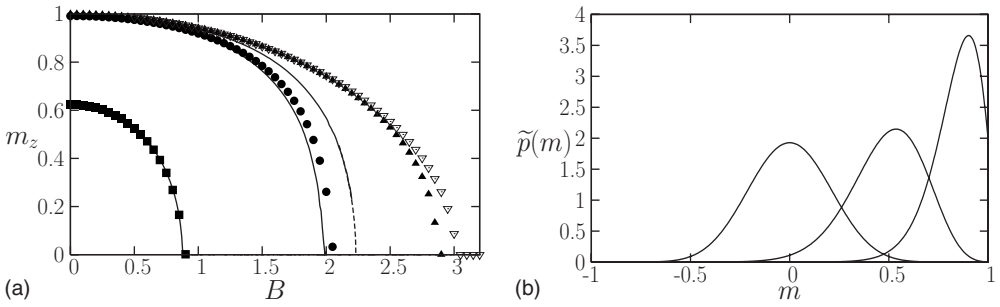

FIG. 9. (a) Longitudinal magnetization m_z as a function of the transverse field B. The full lines are the exact results reported in Fig. 4 for $T=1.7, 1.0, 0.1$ (from left to right). Points are the results of the static approximation: $T=1.7$ (squares), $T=1.0$ (circles), $T=0.1$ (triangles), and $T=0$ (open triangles). (b) The function $\tilde{p}(m)$ defined in the text at temperature $T=0.1$ and transverse field $B=3.2, 2.2, 1.2$ (from left to right). For smaller values of B, the maximum approaches $m=1$ and the weight of the $\delta(m-1)$ starts to increase until $\tilde{p}(m)$ vanishes at $B=0$.

static approximation is obviously exact in the classical case. For a given temperature $T<T_c(B=0)$, we initialized $p(m)$ on the classical solution and increased gradually the transverse field B at each step iterating Eq. (42) until convergence (typically after $\sim 10^2$ iterations with a discretization step $dm \sim 10^{-3}$).

Equation (42) can be further simplified in the limit $T \to 0$. As $I_1(x) \sim e^x$ for large x, the Dirac distributions can be neglected in Eq. (40) for any $B>0$ and at the leading exponential order $w_s(m) \sim e^{\beta B\sqrt{1-m^2}}$. We can thus use the simplified expressions $p(m) \sim e^{\beta\zeta(m)}$, $z_l \sim e^{-\beta e_l}$ at this order, and hence obtain from Eq. (42)

$$\zeta(m) = e_l + B\sqrt{1-m^2} + l \max_{m'}[mm' + \zeta(m')], \qquad (43)$$

where the normalization e_l must be determined in such a way that $\max_m \zeta(m)=0$. Like Eq. (42), the latter equation can be solved iteratively. In this case a good starting guess is $\zeta_0(m)=B\sqrt{1-m^2}+h_0 m+\text{const}$, where the symmetry $m \to -m$ is initially broken by the term $h_0 m$ (with h_0 reasonably small) in order to select one state. Also in this case we used a discretization step $dm \sim 10^{-3}$ and observed convergence after $\sim 10^2$ iterations.

The results of the static approximation are reported in Fig. 9. In the left panel we compared m_z obtained from the static approximation with the exact one obtained by the continuous-time solution of the cavity equation. As expected the approximation is very good for $T \gtrsim 1$ and becomes poor close to $T=0$. Still, the qualitative prediction of the static approximation remains reliable down to $T=0$ even if the value of $B_c^{\text{static}}(T=0)=3.0$ predicted by the static approximation is different from the exact one, $B_c(T=0)=2.232$. In the right panel of Fig. 9 we show the typical shape of $p(m)$: it is a symmetric function at large B, where $a_\pm=0$. On lowering B below B_c^{static}, the distribution becomes asymmetric and $a_+ > a_- > 0$ even if $a_\pm$ remain very small at intermediate B. On approaching $B=0$, $a_\pm$ grow faster and $\tilde{p}(m)$ vanishes until the classical solution is recovered.

In summary, the static approximation is a reliable variational tool to study qualitatively the phase diagram of the system. Remarkably, it can be solved down to $T=0$ (the solution at $T=0$ being easier than for finite T).

IV. QUANTUM MONTE CARLO SIMULATIONS

A. Methods and algorithms

The quantum Monte Carlo method is an important tool that is widely used to study quantum statistical physics and quantum phase transitions, especially in the context of lattice models.[47] In this section, we discuss the application of the ideas discussed in this paper to quantum Monte Carlo simulations.

1. Generic quantum heat-bath Monte Carlo scheme

The procedure we discussed in Sec. II B to generate the "continuous-time" spin configurations can be actually used directly as a *continuous-time quantum heat-bath algorithm*. Once the procedure that generates the new continuous-time configuration given the local-field trajectory is available, the implementation of the Monte Carlo simulation is rather straightforward: one just randomly picks a site, computes the local-field trajectory due to its neighboring spins, and generates a new imaginary-time trajectory of this spin according to the rules discussed in Sec. II B.

The advantage of this method is that one can apply it to *any* discrete spin models on any kind of lattice. In the case of ferromagnetic nonfrustrated interactions, there exist of course a number of algorithms that allow us to considerably speed up the simulation and this is the subject of Sec. IV A 2. However, for highly disordered and frustrated systems such as spin glasses, for instance, no such *generic* cluster algorithm exists even at the classical level [although interesting progresses are being made (see Refs. 48–51)] and most classical simulations[52] rely on the Metropolis or the heat-bath algorithm and the parallel tempering technique.[53] In the case of quantum spin glasses, to the best of our knowledge, only the usual discrete time Suzuki-Trotter decomposition has been tried.[54–56] Another important case where no loop algorithm is known is the one of multispin interactions, where the problems are defined on a factor graph (see Sec. V), which is very common in the context of constraint satisfaction problems such as satisfiability or in coding theory. There is thus a clear need of an efficient generic heat-bath strategy when no cluster or loop algorithm exists, which would result in a substantial gain of simulation time.

In Fig. 10, we show the first application of our continuous-time quantum heat-bath algorithm to the case of

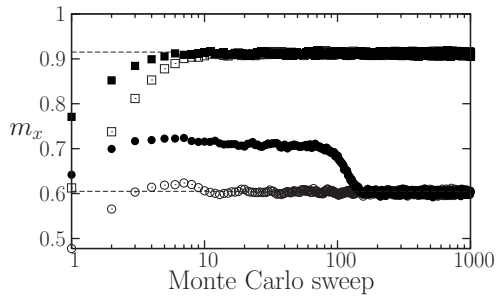

FIG. 10. Quantum heat bath (full symbols) vs loop algorithm (open symbols) for a random regular graph of degree 3 with 10^5 spins at $B=1.6$ (circles), in the ferromagnetic phase, and $B=2.6$ (squares), in the quantum paramagnetic phase, for $T=1$. Dashed lines correspond to the values computed with the cavity method.

the ferromagnetic model on a regular random graph of connectivity 3, as studied in the rest of the present paper. The results of our algorithm converge fastly, with respect to the number of Monte Carlo sweeps, to the asymptotic ones for very large samples (i.e., $N=10^5$ spins). In the paramagnetic phase, the convergence is even *faster* than for the loop algorithm that will be discussed in Sec. IV A 2. The application of these ideas and methods to more complex models is an interesting direction of study.

2. Continuous-time loop algorithm

Since we are dealing with a ferromagnetic nonfrustrated model, we expect the usual cluster and loop algorithms[36,39,57] to allow for a significant speed up of the simulation with respect to the heat-bath procedure even on random graphs. We have thus implemented the algorithms devised by Rieger and Kawashima in Ref. 38, which is an adaptation of the classical Swendsen-Wang[58] algorithm to quantum systems in continuous time. The results are compared with the heat-bath method in Fig. 10. Indeed, the loop algorithm performs very well and better than the heat-bath method close and below the critical point, and we thus have used this method to compare the results of the cavity approach with finite-size instances.

B. Cavity method versus simulation

How does the cavity predictions compare with numerical simulations? To answer this question, we have performed quantum Monte Carlo simulations on random regular graphs of N spins and connectivity 3. For large N we expect the results to be self-averaging and thus we always consider a single instance and do not perform averages of many realizations. The results for two different temperature $T=1$ and $T=0.1$ are shown in Fig. 11 where we plot the longitudinal and transverse magnetizations as a function of B for different sizes from $N=64$ to $N=2048$. The agreement with the asymptotic cavity result is perfect [apart from finite-size effects in m_z for $B \approx B_c$ (see next paragraph)]: this demonstrates the correctness of the approach we have developed in the present paper.

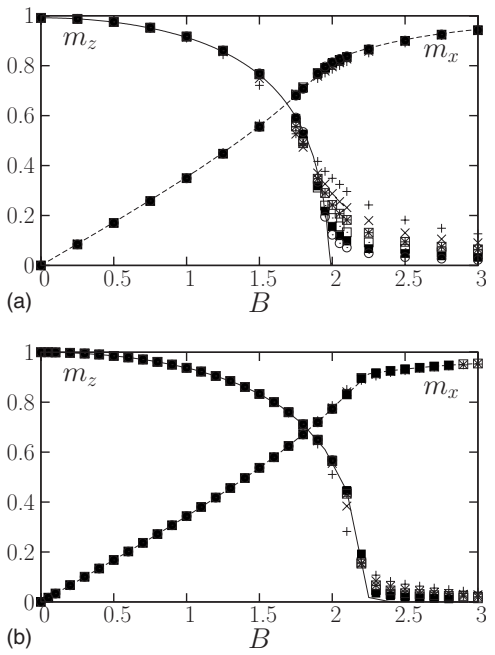

FIG. 11. Longitudinal and transverse magnetization curves for temperatures $T=1$ (top) and $T=0.1$ (bottom). Continuous-time cavity method (m_z—solid line and m_x—dashed line) vs Monte Carlo simulations for different sizes increasing from the top to the bottom ($N=64,128,\ldots,2048$). For the largest size the agreement with the cavity result is excellent (except close to the critical point).

C. Finite size scaling and critical exponent

The transition between the ferromagnetic and the paramagnetic phases is of second order; below the threshold $B_c(T)$ the longitudinal magnetization grows with an exponent β, i.e., $m_z \propto (B_c - B)^{\beta}$, in the thermodynamic limit. We have used finite-size scaling techniques[59,60] to analyze our data in the neighborhood of the transition and to check the mean-field value of the exponent $\beta=1/2$. Let us first briefly recall the basic idea of the finite-size scaling method and the way in which it has to be amended for mean-field models.

In a generic infinite size d-dimensional model, in the vicinity of a second-order phase transition driven by a parameter denoted B, the correlation length diverges as $\xi \propto |B - B_c|^{-\nu}$. For a system of finite extent L the observables depend on the size through a scaling function of the ratio L/ξ. This has to be corrected for dimensions d larger than the upper critical dimension d_u of the considered universality class or when the model lacks any underlying finite-dimensional structure. In that case the scaling function is found[61–65] to depend on the size N (total number of degrees of freedom, equivalent to L^d of a d-dimensional model) through $N^{1/(d_u \nu)}(B - B_c)$, where ν takes its mean-field value in the universality class under investigation. More explicitly the scaling forms of the longitudinal magnetization and of the Binder cumulant $g = \frac{1}{2}\left(3 - \frac{\langle m_z^4 \rangle}{\langle m_z^2 \rangle^2}\right)$ read

$$m_z(B,N) = N^{-\beta/d_u \nu} \tilde{m}[N^{1/(d_u \nu)}(B - B_c)],$$

$$g(B,N) = \tilde{g}[N^{1/(d_u \nu)}(B - B_c)]. \quad (44)$$

We present in Fig. 12 the results of such an analysis for our Monte Carlo data obtained at temperature $T=1$. At this

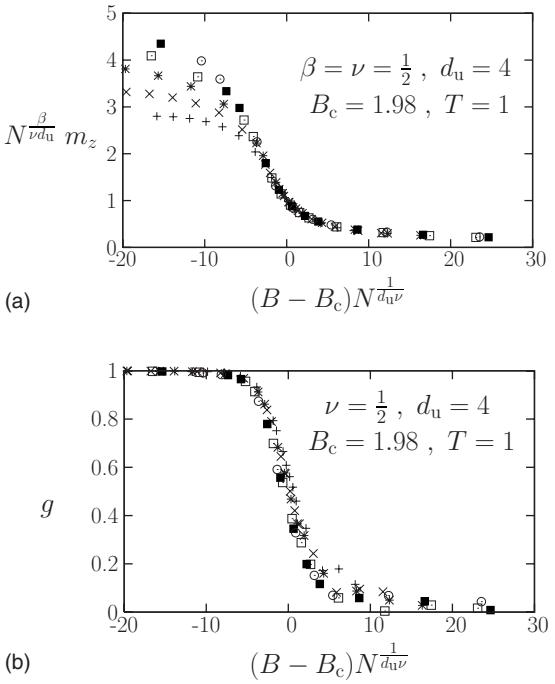

FIG. 12. Finite size scaling analysis of the Monte Carlo data. Top: rescaling of the longitudinal magnetization for random graphs of different sizes (increasing from the top to the bottom) $N=64,128,\ldots,2048$. Bottom: Binder parameter for the same sizes.

positive temperature the critical behavior of a quantum d-dimensional system is equivalent to a classical d-dimensional Ising model,[13,29] which implies $d_u=4$ and $\nu=1/2$. Using the cavity method predictions $B_c(T=1)=1.98$ and $\beta=1/2$ we found a very good data collapse (see Fig. 12), which confirms the validity of these values of β and B_c.

To close this section, let us discuss the value of the critical exponent β at $T=0$. We believe that because of the mean-field nature of the Bethe lattice model, β keeps the same value 1/2 at positive and zero temperatures. This is indeed what happens for the Curie-Weiss model (see Appendix A). A simple argument is the following. For ferromagnetic models the Suzuki-Trotter formalism and numerical simulations suggest that the critical behavior of the quantum d-dimensional model at zero temperature corresponds to the one of the classical model in $d+1$ dimensions.[13,29,38] Hence if a model behaves in a mean-field way at positive temperature it should also do so at zero temperature, having formally gained one more spatial dimension. To give further credit to our theses we performed quantum Monte Carlo simulations at very small temperatures, $T=0.01$. The plot of Fig. 13 shows again a very good collapse with the value $\beta=1/2$ using the zero-temperature critical value of the transverse field extracted from the cavity computation, $B_c=2.232$. This collapse has been obtained with $d_u=3$; indeed at such a low temperature we are well inside the low-temperature regime where the transition is truly quantum, hence the shift of the upper critical dimension to account for the imaginary-time supplementary dimension.

A different value of the zero-temperature exponent, $\beta=0.41$, has been obtained in Ref. 24 using the matrix product state ansatz for the description of the ground state. Though

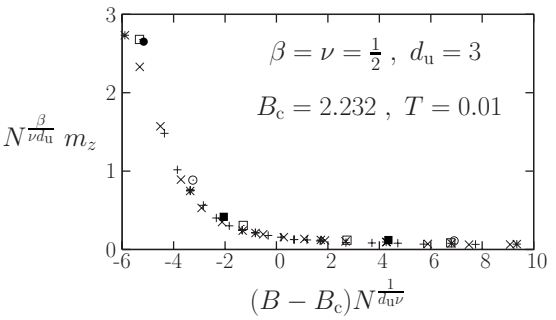

FIG. 13. Finite size scaling analysis of the longitudinal magnetization at $T=0.01$ for sizes $N=32,64,\ldots,2048$.

we cannot rule out the possibility that a crossover occurs at temperatures even lower than $T=0.01$, we believe that $\beta=1/2$ down to $T=0$, in accordance with the mean-field nature of the Bethe lattice, and that the different values reported in Ref. 24 might be due to the truncation of the matrix product state ansatz.

V. GENERIC REPLICA SYMMETRIC QUANTUM CAVITY METHOD

In this final section we give a more generic description of the replica symmetric quantum cavity method. As the main ideas should have already been conveyed by the example of the ferromagnet on the random regular graphs we shall mainly emphasize the differences and complications that arise in more general models.

Let us consider the class of Ising spin models whose classical energy $E(\underline{\sigma})$ can be decomposed into the sum of M interaction terms $a=1,\ldots,M$, each of them depending on a finite number of spins,

$$E(\underline{\sigma}) = \sum_{a=1}^{M} \varepsilon(\underline{\sigma}_{\partial a}, J_a). \tag{45}$$

In this expression ∂a is the subset of spin indices the ath interaction effectively depends on, $\underline{\sigma}_{\partial a}=(\sigma_i : i \in \partial a)$ is a shorthand for the configuration of those spins, and J_a denotes coupling constants that might appear in the definition of the ath interaction term. This decomposition is conveniently represented as a factor graph,[44] i.e., a graph with two kinds of vertices (see Fig. 14 for an illustration): squares stand for the interactions $a=1,\ldots,M$, while circles represent the variables $i=1,\ldots,N$. An edge is drawn between an interaction a and a variable i whenever a depends on i, in other words whenever $i \in \partial a$. In this graphical representation ∂a is thus the set of nodes adjacent to a. Similarly we shall denote ∂i the set of neighbors of i, which is all the interactions that depend on σ_i. The extended Ising model defined in Eq. (5) preserves the topology of the interactions of the classical energy $E(\underline{\sigma})$, the latter being reproduced identically in the various imaginary-time slices,

$$\tilde{E}(\underline{\boldsymbol{\sigma}}) = \sum_{a=1}^{M} \tilde{\varepsilon}(\underline{\boldsymbol{\sigma}}_{\partial a}, J_a),$$

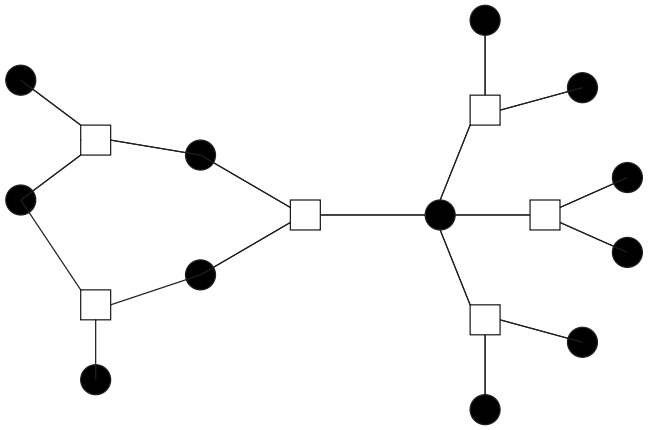

FIG. 14. An example of a factor graph.

$$\tilde{\varepsilon}(\underline{\boldsymbol{\sigma}}_{\partial a}, J_a) = \frac{1}{N_s}\sum_{\alpha=1}^{N_s} \varepsilon(\underline{\sigma}_{\partial a}^{\alpha}, J_a), \tag{46}$$

while the transverse weights $w(\boldsymbol{\sigma}_i)$ are local in the spin indices i.

As we did on the ferromagnet example we first state the solution of this extended model on a tree. The difference is that we have now two kinds of messages from variables to interactions and vice versa. Let us denote $\mu_{a\to i}(\boldsymbol{\sigma}_i)$ the probability law of $\boldsymbol{\sigma}_i$ in the model corresponding to the factor graph where all interactions but a have been removed in the neighborhood of i and similarly $\mu_{i\to a}(\boldsymbol{\sigma}_i)$ for the factor graph with only a removed from ∂i. These quantities obey the following recursion equations,

$$\mu_{i\to a}(\boldsymbol{\sigma}_i) = \frac{1}{z_{i\to a}} w(\boldsymbol{\sigma}_i) \prod_{b\in\partial i\backslash a} \mu_{b\to i}(\boldsymbol{\sigma}_i),$$

$$\mu_{a\to i}(\boldsymbol{\sigma}_i) = \frac{1}{z_{a\to i}} \sum_{\{\boldsymbol{\sigma}_j\}_{j\in\partial a\backslash i}} e^{-\beta\tilde{\varepsilon}(\underline{\boldsymbol{\sigma}}_{\partial a}, J_a)} \prod_{j\in\partial a\backslash i} \mu_{j\to a}(\boldsymbol{\sigma}_j), \tag{47}$$

on all edges of the factor graph, the various constants z being normalization factors. The reader will easily verify that these equations reduce to Eq. (23) in the ferromagnetic case with $\varepsilon(\sigma_i,\sigma_j)=-\sigma_i\sigma_j$; in this case we could eliminate one type of message (from interactions to variables) as the interactions were only pairwise.

We shall now consider ensembles of random factor graphs, denoting $\mathbb{E}[\cdot]$ the expectation over the distribution of the graphs and coupling constants. We assume all interaction nodes to involve a fixed number k of variables (the ferromagnet corresponded to $k=2$), while the degree distribution of the variables is specified by a probability law q_d over the positive integers (all random graphs verifying these constraints are equiprobable in the ensemble; the lack of a finite-dimensional *a priori* structure is the origin of the mean-field character of this family of models). We shall denote $\gamma k = \sum_d d q_d$ the average variable degree. Moreover the $M=\gamma N$ coupling constants J_a are drawn in an identical independent way for each of the interactions. Suppose the recursion [Eq. (47)] is solved on a factor graph sampled at random from the ensemble under consideration and that an edge from a variable to an interaction, call it $i\to a$, is chosen uniformly at random. The probability law $\mu_{i\to a}$ it bears is itself a random variable, denoted η in the following, due to the random choices of the graph and of its coupling constants. This random variable can be related to its neighboring equivalents by the local relations [Eq. (47)]. Suppose that i has d adjacent interactions apart from a (see Fig. 15 for an illustration). Then one has, from Eq. (47),

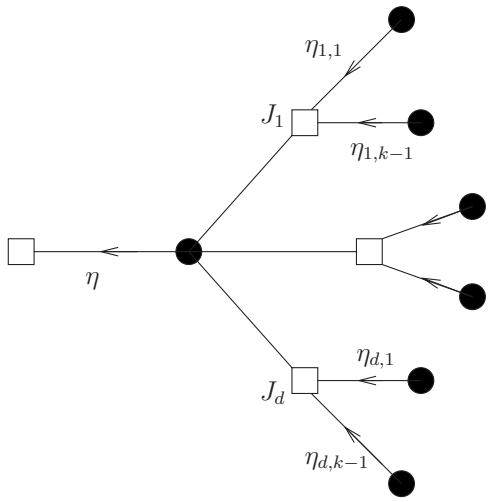

FIG. 15. A pictorial representation of Eq. (48).

$$\eta(\boldsymbol{\sigma}) = \frac{1}{z} w(\boldsymbol{\sigma}) \sum_{\substack{\{\boldsymbol{\sigma}_{a,i}\}_{a\in[1,d]}^{i\in[1,k-1]}}} \left(\prod_{a,i} \eta_{a,i}(\boldsymbol{\sigma}_{a,i})\right) \times \exp\left(-\beta\sum_{a=1}^{d} \tilde{\varepsilon}(\boldsymbol{\sigma}, \boldsymbol{\sigma}_{a,1}, \ldots, \boldsymbol{\sigma}_{a,k-1}, J_a)\right), \tag{48}$$

where the $\eta_{a,i}$ are the $d(k-1)$ probability laws that determine η. The hypothesis of the replica symmetric cavity method is to assume that the above form is correct in spite of the graph not being globally a tree and that the $\eta_{a,i}$ are independent identically distributed copies of the random variable η, which is written in formula as

$$\eta \overset{d}{=} f(\eta_{1,1}, \ldots, \eta_{1,k-1}, \ldots, \eta_{d,1}, \ldots, \eta_{d,k-1}, J_1, \ldots, J_d), \tag{49}$$

the symbol $\overset{d}{=}$ denoting identity in distribution of random variables and the function f being an abbreviation of the right-hand side of Eq. (48). Note that the connectivity random variable d is not distributed according to q_d but rather $\tilde{q}_d=(d+1)q_{d+1}/\gamma k$: as one uniformly chose a random edge of the graph and not a random site, this sampling favors larger connectivity variables. For the ferromagnet on the random regular graph one had $q_d=\delta_{d,l+1}$ while $\tilde{q}_d=\delta_{d,l}$.

The physical observables of the system can be computed from the solution of this distributional equation. The thermodynamic limit of the free-energy per site is found to be

$$
\begin{aligned}
-\beta f &= \lim_{N\to\infty}\frac{1}{N}\mathbb{E}[\ln Z] \\
&= \mathbb{E}\Bigg[\ln\Bigg\{\sum_{\boldsymbol{\sigma},\{\boldsymbol{\sigma}_{a,i}\}_{a\in[1,d]}^{i\in[1,k-1]}}\Bigg[\prod_{a,i}\eta_{a,i}(\boldsymbol{\sigma}_{a,i})\Bigg]w(\boldsymbol{\sigma}) \\
&\quad\times\exp\Bigg[-\beta\sum_{a=1}^{d}\tilde{\varepsilon}(\boldsymbol{\sigma},\boldsymbol{\sigma}_{a,1},\ldots,\boldsymbol{\sigma}_{a,k-1},J_a)\Bigg]\Bigg\}\Bigg] \\
&\quad-\gamma(k-1)\mathbb{E}\Bigg[\ln\Bigg\{\sum_{\boldsymbol{\sigma}_1,\ldots,\boldsymbol{\sigma}_k}\Bigg[\prod_{i}\eta_i(\boldsymbol{\sigma}_i)\Bigg]e^{-\beta\tilde{\varepsilon}(\boldsymbol{\sigma}_1,\ldots,\boldsymbol{\sigma}_k,J)}\Bigg\}\Bigg],
\end{aligned}
\tag{50}
$$

where the expectations of the left-hand side are over the choice of the random factor graphs and for the right-hand side over independent copies of the random variable η and the coupling constants J, while in the first term d is drawn from the law q_d. This is a generalization of expression (30) found for the ferromagnet. Similarly the average marginal of law (5) for an arbitrary site reads

$$
\begin{aligned}
\mu(\boldsymbol{\sigma}) &= \mathbb{E}\Bigg\{\frac{1}{z}w(\boldsymbol{\sigma})\sum_{\{\boldsymbol{\sigma}_{a,i}\}_{a\in[1,d]}^{i\in[1,k-1]}}\Bigg[\prod_{a,i}\eta_{a,i}(\boldsymbol{\sigma}_{a,i})\Bigg] \\
&\quad\times\exp\Bigg[-\beta\sum_{a=1}^{d}\tilde{\varepsilon}(\boldsymbol{\sigma},\boldsymbol{\sigma}_{a,1},\ldots,\boldsymbol{\sigma}_{a,k-1},J_a)\Bigg]\Bigg\}
\end{aligned}
\tag{51}
$$

with d drawn from q_d, while the average marginal law of the k variables in an arbitrary interaction is

$$
\mu(\boldsymbol{\sigma}_1,\ldots,\boldsymbol{\sigma}_k) = \mathbb{E}\Bigg[\frac{1}{z}\Bigg(\prod_i\eta_i(\boldsymbol{\sigma}_i)\Bigg)e^{-\beta\tilde{\varepsilon}(\boldsymbol{\sigma}_1,\ldots,\boldsymbol{\sigma}_k,J)}\Bigg], \tag{52}
$$

the factors $1/z$ in these last two equations ensuring their normalization [cf. Eq. (31) for the regular ferromagnet].

Let us now discuss a method of resolution of the distributional equation [Eq. (49)], consisting in encoding the distribution of η by a sample (or population) of a large number $\mathcal{N}$ of representatives η_i. From an arbitrarily initialized population, one applies iteration steps according to Eq. (49): one draws an integer d from $\tilde{q}_d$, d coupling constants $J_1,\ldots,J_d$, and $d(k-1)$ indices in $[1,\mathcal{N}]$. The right-hand side of Eq. (49) is then computed from the corresponding $d(k-1)$ representants of η randomly chosen in the population, and the resulting η is used to replace one discarded element of the population. The iteration of these steps brings the population close to a fixed point of the distributional equation; then physical observables such as the average free energy [see Eq. (50)] can be computed, evaluating the expectations over the random variable η as a sampling from the approximate representation provided by the finite population. Compared with the classical replica symmetric cavity method the difficulty is that each of the η_i in this population is itself a probability distribution over configurations of spin rings or in the continuous limit over spin trajectories. It is however possible to apply the trick explained in the simpler case of the ferromagnet and encode each of the η_i as a sample of $\mathcal{N}_{\text{traj}}$ spin trajectories. Let us introduce some further notations in order to give an explicit form of the updating procedure of the population of η_i's.

The dependence of $\varepsilon(\cdot,J)$ on one of the Ising spins can always be parametrized through two functions u and v as

$$
\begin{aligned}
\varepsilon(\sigma,\sigma_1,\ldots,\sigma_{k-1},J) &= -\sigma u(\sigma_1,\ldots,\sigma_{k-1},J) \\
&\quad + v(\sigma_1,\ldots,\sigma_{k-1},J),
\end{aligned}
\tag{53}
$$

u playing the role of an effective magnetic field acting on σ. For N_s-fold replicated variables we define

$$
\begin{aligned}
&\boldsymbol{u}(\boldsymbol{\sigma}_1,\ldots,\boldsymbol{\sigma}_{k-1},J) \\
&\quad= (u(\sigma_1^1,\ldots,\sigma_{k-1}^1,J),\ldots,u(\sigma_1^{N_s},\ldots,\sigma_{k-1}^{N_s},J)),
\end{aligned}
\tag{54}
$$

$$
\tilde{v}(\boldsymbol{\sigma}_1,\ldots,\boldsymbol{\sigma}_{k-1},J) = \frac{1}{N_s}\sum_{\alpha=1}^{N_s}v(\sigma_1^\alpha,\ldots,\sigma_{k-1}^\alpha,J). \tag{55}
$$

Using the definitions in Eq. (32), we can then rewrite Eq. (48) as

$$
\begin{aligned}
\eta(\boldsymbol{\sigma}) &= \sum_{\{\boldsymbol{\sigma}_{a,i}\}_{a\in[1,d]}^{i\in[1,k-1]}}\Bigg[\prod_{a,i}\eta_{a,i}(\boldsymbol{\sigma}_{a,i})\Bigg]p\{\boldsymbol{\sigma}|\boldsymbol{h}[(\boldsymbol{\sigma}_{a,i},J_a)]\} \\
&\quad\times\frac{z[(\boldsymbol{\sigma}_{i,a},J_a)]}{z},
\end{aligned}
\tag{56}
$$

$$
\boldsymbol{h}[(\boldsymbol{\sigma}_{a,i},J_a)] = \sum_{a=1}^{d}\boldsymbol{u}(\boldsymbol{\sigma}_{a,1},\ldots,\boldsymbol{\sigma}_{a,k-1},J_a),
$$

$$
\begin{aligned}
z[(\boldsymbol{\sigma}_{a,i},J_a)] &= \mathcal{Z}\{\boldsymbol{h}[(\boldsymbol{\sigma}_{a,i},J_a)]\} \\
&\quad\times\exp\Bigg[-\beta\sum_{a=1}^{d}\tilde{v}(\boldsymbol{\sigma}_{a,1},\ldots,\boldsymbol{\sigma}_{a,k-1},J_a)\Bigg].
\end{aligned}
$$

We can thus apply the sampling procedure explained in Sec. III B, the only change being the different definition of the effective-field trajectory $\boldsymbol{h}$ and the inclusion of a contribution arising from the function v in the weights of the generated spin trajectories. Let us emphasize that at variance with the classical cavity method, here we have to deal with a population of population of spin trajectories (of total size $\mathcal{N}\times\mathcal{N}_{\text{traj}}$) already at the replica symmetric level.

VI. CONCLUSIONS

The explicit procedure for the construction of continuous-time spin trajectories presented in Sec. II B allowed us to make progresses both on the analytical side, with an improvement over the discretized time cavity method in Ref. 21 and the static approximation in Ref. 23, and on the numerical simulations side, with a generic quantum Monte Carlo procedure for spin-1/2 models in transverse field. The ferromagnetic model we studied in this paper is only the simplest of a large family that can be tackled, at the price of a heavier computational cost, with the same methods. We believe that its study was in any case worthwhile from a methodological point of view: its simplicity permitted a complete resolution of the quantum cavity equations, which (i) showed a perfect

agreement with Monte Carlo simulations, hence giving credit to the conjecture that the replica symmetric cavity method leads to exact results in the thermodynamic limit for sparse mean-field ferromagnetic systems, as was proved for classical models in Ref. 46 and (ii) allowed us to test quantitatively some approximate treatments (finite N_s and static approximation).

The more interesting cases we plan to address in the future by means of the cavity method will involve fluctuating connectivities in order to study the role of these local fluctuations on the critical behavior of the models, glassy phases at low temperatures (a particularly motivating case will be the regular multispin ferromagnet studied at the classical level in Ref. 66), and models related to quantum computing issues as the random k-satisfiability model in a transverse field.[23] Note that already the replica symmetric treatment of these models will involve a population of populations of spin trajectories, as explained in Sec. V, which will make an exact treatment of the one-step replica-symmetry-breaking version of the cavity method extremely challenging. We hope however that the better control of the approximative treatments we gained on the simple ferromagnet will help us to devise appropriate approximate strategies to handle these cases.

At the same time, we proposed a heat-bath Monte Carlo strategy that should be applicable to general spin-1/2 models. The performance of this algorithm should be tested on frustrated models for which cluster algorithms are not easy to implement, and we expect that in such cases the heat-bath method could give interesting results.

The strategy developed above becomes inefficient at very low temperatures because the spins jump many times along a trajectory and the amount of information needed to encode $\eta(\boldsymbol{\sigma})$ by a population of trajectories becomes very large. Therefore the important directions of research would be to look for possible simplifications of the formalism in the limit $\beta \to \infty$. Moreover, one could use the recursion equations [Eq. (47)] on a given sample, thus constructing a quantum belief propagation algorithm.[67] Finally, it is worth noting that the procedure described in Sec. II B, on which our results are based, is in principle not restricted to spin-1/2 models. It should be possible to generalize it to any model built on discrete degrees of freedom,[30] for instance, hard-core bosons or higher spin models.

ACKNOWLEDGMENTS

We wish to thank G. Biroli, W. Krauth, M. Mézard, M. Müller, H. Rieger, A. Scardicchio, S. Sondhi, P. Young, M. Tarzia, and L. Zdeborová for discussions and comments on a first version of the paper.

APPENDIX A: QUANTUM CURIE-WEISS MODEL

This appendix is devoted to a study of the simplest quantum mean-field ferromagnet, namely, the fully connected Curie-Weiss quantum model.[68–70] The model is defined by the Hamiltonian

$$\hat{H} = -\frac{J}{2N}\sum_{i,j=1}^{N}\sigma_i^z\sigma_j^z - B\sum_{i=1}^{N}\sigma_i^x - h\sum_{i=1}^{N}\sigma_i^z, \tag{A1}$$

where the scaling of the coupling constant is chosen appropriately to make the thermodynamic limit well defined. At variance with the Bethe lattice model here each spin interacts with all others. Applying the Suzuki-Trotter decomposition described in Sec. II A leads for a finite number N_s of Suzuki-Trotter slices to the following expression of the partition function:

$$Z = \sum_{\underline{\boldsymbol{\sigma}}}\left(\prod_{i=1}^{N} w(\boldsymbol{\sigma}_i)\exp\left[\frac{\beta h}{N_s}\sum_{\alpha=1}^{N_s}\sigma_i^\alpha\right]\right) \times \exp\left[\frac{\beta J}{2NN_s}\sum_{\alpha=1}^{N_s}\sum_{i,j=1}^{N}\sigma_i^\alpha\sigma_j^\alpha\right]. \tag{A2}$$

We then perform N_s Hubbard-Stratanovitch transformations to disentangle the quadratic terms and obtain

$$Z = \left(\frac{\beta JN}{2\pi N_s}\right)^{N_s/2}\int\prod_{\alpha=1}^{N_s}dm^\alpha \exp\left[-N\frac{\beta J}{2}\frac{1}{N_s}\sum_{\alpha=1}^{N_s}(m^\alpha)^2 + N\ln \mathrm{Tr}\left(\prod_{\alpha} e^{(\beta/N_s)(h+Jm^\alpha)\sigma^z}e^{(\beta/N_s)B\sigma^x}\right)\right]. \tag{A3}$$

Evaluating these integrals by the saddle-point method in the thermodynamic limit and selecting the cyclically invariant saddle point yield

$$\lim_{N\to\infty}\frac{1}{N}\ln Z = \sup_m\left[-\frac{\beta J}{2}m^2 + \ln \mathrm{Tr}((e^{(\beta/N_s)(h+Jm)\sigma^z}e^{(\beta/N_s)B\sigma^x})^{N_s})\right]. \tag{A4}$$

This can be further simplified if the $N_s \to \infty$ limit is performed afterward and yields for the free-energy per site,

$$f = \inf_m\left[\frac{J}{2}m^2 - \frac{1}{\beta}\ln\{2\cosh[\beta\sqrt{(h+Jm)^2+B^2}]\}\right]. \tag{A5}$$

Using the variational character of this expression the longitudinal and transverse magnetizations (i.e., m_z and m_x) can be obtained by taking the explicit derivatives with respect to h and B, respectively,

$$m_z \equiv \langle\sigma_i^z\rangle = \frac{h+Jm}{\sqrt{(h+Jm)^2+B^2}}\tanh(\beta\sqrt{(h+Jm)^2+B^2}), \tag{A6}$$

$$m_x \equiv \langle\sigma_i^x\rangle = \frac{B}{\sqrt{(h+Jm)^2+B^2}}\tanh(\beta\sqrt{(h+Jm)^2+B^2}), \tag{A7}$$

where m is taken as the solution of the saddle-point equation. The latter is easily found to imply that $m=m_z$ at the saddle point. In the following we take $J=1$ to simplify the notations.

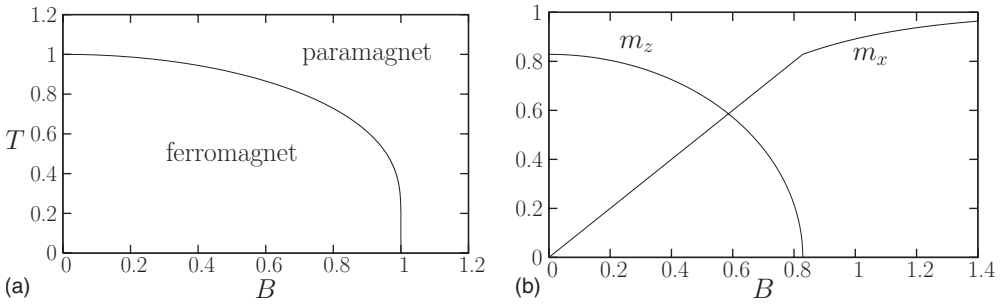

FIG. 16. (a) The phase diagram of the quantum Curie-Weiss model. (b) Longitudinal and transverse magnetizations as a function of the transverse field for $T=0.7$.

In absence of the transverse field ($B=0$) one recovers the classical Curie-Weiss model, with $m=m_{\rm cl}(\beta,h)$ solution of the traditional equation $m=\tanh[\beta(m+h)]$. The ferromagnetic transition is signaled by the appearance of a nontrivial solution at $h=0$, which is possible for small enough temperatures, i.e., for $\beta>\beta_c(B=0)=1$.

Consider now the solutions of the saddle-point equation with $B>0$ and $h=0$. The paramagnetic solution $m=0$ exists for all temperatures and transverse fields. For a strictly positive solution m the saddle-point equation reduces to $\sqrt{m^2+B^2}=\tanh(\beta\sqrt{m^2+B^2})$, that is, $m(\beta,B,h=0)=\sqrt{m_{\rm cl}(\beta,h=0)^2-B^2}$. This is possible only for small enough temperatures and transverse fields, such that the argument of the square root remains positive. The line of transition in the (B,T) plane is such that $B_c(\beta)=m_{\rm cl}(\beta,h=0)$ (see the top panel of Fig. 16). Note the vertical slope of the transition line in the neighborhood of the quantum critical point in $(B=1,\ T=0)$; in fact, one can perform an asymptotic expansion in this region to show that

$$B_c(T) \underset{T\to 0}{\sim} 1-2e^{-2\beta} \tag{A8}$$

or equivalently

$$T_c(B) \underset{B\to 1}{\sim} \frac{1}{\ln\left(\frac{1}{\sqrt{1-B}}\right)}. \tag{A9}$$

The bottom panel of Fig. 16 shows the evolution, as a function of the transverse field, of the longitudinal and transverse magnetizations at a temperature smaller than the classical critical temperature $T_c(B=0)=1$. The transverse magnetization is continuous but its derivative has a finite jump at the transition. One can indeed show from Eq. (A7) that $m_x=B$ in the ferromagnetic phase, while $m_x=\tanh(\beta B)$ for the paramagnetic one.

Another thermodynamic quantity easily computed for the Curie-Weiss model is the ground-state energy per spin, $e_{\rm GS}(B)$, obtained from Eq. (A5) in the limit $\beta\to\infty$. One finds

$$e_{\rm GS}(B)=\begin{cases} -\frac{1}{2}(1+B^2) & \text{for } B\le B_c=1 \\ -B & \text{for } B\ge B_c=1, \end{cases} \tag{A10}$$

which shows that $e_{\rm GS}(B)$ and its first derivative are continuous at the transition, while its second derivative has a finite jump.

Let us finally argue about the scaling of the finite N_s corrections, reconsidering the step we took between Eqs. (A4) and (A5). At the next-to-leading order one would have obtained

$$\begin{aligned}\mathrm{Tr}\{[e^{(\beta/N_s)(h+Jm)\sigma^z}e^{(\beta/N_s)B\sigma^x}]^{N_s}\} &= \mathrm{Tr}\Bigg(\exp\Bigg[\beta(h+Jm)\sigma^z+\beta B\sigma^x \\ &\quad +\frac{1}{2N_s}\beta^2 B(h+Jm)(\sigma^z,\sigma^x)\Bigg][1+O(N_s^{-2})]\Bigg).\end{aligned} \tag{A11}$$

One can then check explicitly that the eigenvalues of the matrix in the exponential are not modified at the order N_s^{-1}, hence the finite N_s correction on the observables should be of order N_s^{-2}, as we observed in the study of the Bethe lattice ferromagnet.

APPENDIX B: AN IDENTITY IN THE CONTINUOUS-TIME LIMIT

In this appendix we briefly justify the claim made in Sec. III B of the equivalence in the continuous-time limit of the definition of $\mathcal{Z}(\boldsymbol{h})$ given in Eq. (32) with the one of Eq. (20). Before taking the $N_s\to\infty$ limit, the former reads

$$\begin{aligned}\mathcal{Z}(\boldsymbol{h}) &= \sum_{\boldsymbol{\sigma}} w(\boldsymbol{\sigma})\exp[\beta\boldsymbol{\sigma}\cdot\boldsymbol{h}] \\ &= \sum_{\sigma^1,\ldots,\sigma^{N_s}}\prod_{\alpha=1}^{N_s}\langle\sigma^\alpha|e^{(\beta/N_s)h^\alpha\sigma^z}e^{(\beta/N_s)B\sigma^x}|\sigma^{\alpha+1}\rangle.\end{aligned} \tag{B1}$$

We shall denote $N_s^{(i)}=N_s\lambda^{(i)}/\beta$ the lengths of the constant longitudinal field intervals (see Fig. 2), expressed in number of Suzuki-Trotter slices. Then

$$\begin{aligned}\mathcal{Z}(\boldsymbol{h}) &= \sum_{\sigma(t^{(0)}),\ldots,\sigma(t^{(p)})}\prod_{i=1}^{p}\langle\sigma(t^{(i)})|(e^{(\beta/N_s)h^{(i)}\sigma^z}e^{(\beta/N_s)B\sigma^x})^{N_s^{(i)}} \\ &\quad\times|\sigma(t^{(i+1)})\rangle,\quad \sigma(t^{(p+1)})=\sigma(t^{(0)}) \\ &= \sum_{\sigma(t^{(0)}),\ldots,\sigma(t^{(p)})}\prod_{i=0}^{p}\langle\sigma(t^{(i)})|e^{\lambda^{(i)}(h^{(i)}\sigma^z+B\sigma^x)}|\sigma(t^{(i+1)})\rangle.\end{aligned} \tag{B2}$$

In the last step we have taken the $N_s \to \infty$ limit to obtain the expression of Eq. (20).

APPENDIX C: THE COMPUTATION OF $w_s(m)$

In this appendix we derive expression (40) for the average transverse weight in the static approximation. Rewriting the sum over $\boldsymbol{\sigma}$ of Eq. (39) as a sum over paths in the continuous-time limit, one obtains

$$\begin{aligned} w_s(m) &= \sum_{\sigma} \sum_{n=0}^{\infty} B^{2n} \int_0^\beta dt_1 \int_{t_1}^\beta dt_2 \cdots \int_{t_{2n-1}}^\beta dt_{2n} \\ &\quad \times \delta\left(m - \sigma \frac{2t_1 - 2t_2 + \cdots - 2t_n + \beta}{\beta} \right) \\ &= \delta(m-1) + \delta(m+1) + \sum_{\sigma} \sum_{n=1}^{\infty} (B\beta)^{2n} \int_0^1 dx_1 \\ &\quad \times \int_{x_1}^1 dx_2 \cdots \int_{x_{2n-1}}^1 dx_{2n} \\ &\quad \times \delta(2x_1 - 2x_2 + \cdots - 2x_n + 1 - m\sigma), \end{aligned} \tag{C1}$$

where in the second line we have isolated the contribution of the constant trajectories and changed variables from t_i to $x_i = t_i/\beta$. Let us concentrate on the term corresponding to a given value of $n > 0$. We perform a further change in variables, setting $y_i = x_i - x_{i-1}$ (with $x_0 = 0$), the intervals between the reduced time of flips in the trajectory. The Jacobian of this change in variables being 1, the integral over $x_1, \ldots, x_{2n}$ can be rewritten as

$$\begin{aligned} &\int_0^1 dy_1 \cdots dy_{2n} \mathbb{1}(y_1 + y_2 + \cdots + y_{2n} \le 1) \\ &\quad \times \delta[2y_2 + 2y_4 + \cdots + 2y_{2n} - (1 - m\sigma)] \\ &= \frac{1}{2} \int_0^1 dS_o dS_e \rho_n(S_o) \rho_n(S_e) \mathbb{1}(S_o + S_e \le 1) \\ &\quad \times \delta\left(S_e - \frac{1 - m\sigma}{2} \right) \\ &= \frac{1}{2} \rho_n\left(\frac{1 - m\sigma}{2} \right) \int_0^{1 + m\sigma/2} dS \rho_n(S). \end{aligned} \tag{C2}$$

Here we have used $\mathbb{1}(\cdot)$ as the indicator function of an event, $S_o = y_1 + y_3 + \cdots + y_{2n-1}$ and $S_e = y_2 + \cdots + y_{2n}$ the sum of the odd or even y_i's, and $\rho_n(S)$ as the density of the distribution of the sum of n independent random variables uniformly distributed on $[0,1]$. It is easy to prove by recurrence that for $S \in [0,1]$ one has $\rho_n(S) = S^{n-1}/(n-1)!$. Collecting these facts together leads to

$$w_s = \delta(m-1) + \delta(m+1) + \sum_{n=1}^{\infty} \frac{1}{n!\,(n-1)!} \frac{(\beta B)^{2n} (1 - m^2)^{n-1}}{2^{2n-1}}, \tag{C3}$$

which is indeed equal to Eq. (40), thanks to the series expansion of the Bessel function.

[1] R. Abou-Chacra, D. J. Thouless, and P. W. Anderson, J. Phys. C **6**, 1734 (1973).
[2] A. Georges, G. Kotliar, W. Krauth, and M. J. Rozenberg, Rev. Mod. Phys. **68**, 13 (1996).
[3] D. Sherrington and S. Kirkpatrick, Phys. Rev. Lett. **35**, 1792 (1975).
[4] R. J. Baxter, *Exactly Solved Models in Statistical Mechanics* (Academic, New York, 1989).
[5] L. Viana and A. J. Bray, J. Phys. C **18**, 3037 (1985).
[6] M. Mézard and G. Parisi, Eur. Phys. J. B **20**, 217 (2001).
[7] R. Monasson and R. Zecchina, Phys. Rev. E **56**, 1357 (1997).
[8] M. Mézard, G. Parisi, and R. Zecchina, Science **297**, 812 (2002).
[9] F. Krzakala, A. Montanari, F. Ricci-Tersenghi, G. Semerjian, and L. Zdeborová, Proc. Natl. Acad. Sci. U.S.A. **104**, 10318 (2007).
[10] M. Mézard, G. Parisi, and M. A. Virasoro, *Spin Glass Theory and Beyond* (World Scientific, Singapore, 1987).
[11] R. Monasson, J. Phys. A **31**, 513 (1998).
[12] G. Biroli and L. F. Cugliandolo, Phys. Rev. B **64**, 014206 (2001).
[13] S. Sachdev, *Quantum Phase Transitions* (Cambridge University Press, Cambridge, England, 1999).
[14] A. J. Bray and M. A. Moore, J. Phys. C **13**, L655 (1980).
[15] Y. Y. Goldschmidt, Phys. Rev. B **41**, 4858 (1990).
[16] H. Nishimori and Y. Nonomura, J. Phys. Soc. Jpn. **65**, 3780 (1996).
[17] A. Georges, O. Parcollet, and S. Sachdev, Phys. Rev. Lett. **85**, 840 (2000).
[18] L. F. Cugliandolo, D. R. Grempel, and C. A. da Silva Santos, Phys. Rev. B **64**, 014403 (2001).
[19] M. P. Kennett, C. Chamon, and J. Ye, Phys. Rev. B **64**, 224408 (2001).
[20] M. Müller and L. B. Ioffe, arXiv:0711.2668 (unpublished).
[21] C. Laumann, A. Scardicchio, and S. L. Sondhi, Phys. Rev. B **78**, 134424 (2008).
[22] M. Tarzia and G. Biroli, Europhys. Lett. **82**, 67008 (2008).
[23] S. Knysh and V. N. Smelyanskiy, arXiv:0803.0149 (unpublished).
[24] D. Nagaj, E. Farhi, J. Goldstone, P. Shor, and I. Sylvester, Phys. Rev. B **77**, 214431 (2008).
[25] B. Apolloni, N. Cesa-Bianchi, and D. de Falco, in *Stochastic Processes, Physics and Geometry*, Proceedings of the 1988 Ascona-Locarno Conference, Vol. 97, edited by S. Albeverio, G. Casati, U. Cattaneo, D. Merlini, and R. Moresi (World Scientific, Singapore, 1990).
[26] T. Kadowaki and H. Nishimori, Phys. Rev. E **58**, 5355 (1998).
[27] E. Farhi, J. Goldstone, S. Gutmann, J. Lapan, A. Lundgren, and D. Preda, Science **292**, 472 (2001).
[28] T. Jörg, F. Krzakala, J. Kurchan, and A. C. Maggs, Phys. Rev. Lett. **101**, 147204 (2008).

[29] M. Suzuki, Prog. Theor. Phys. **56**, 1454 (1976).
[30] E. Farhi and S. Gutmann, Ann. Phys. (N.Y.) **213**, 182 (1992).
[31] R. P. Feynman, Phys. Rev. **91**, 1291 (1953).
[32] J. Ginibre, Commun. Math. Phys. **10**, 140 (1968).
[33] G. Gallavotti, S. Miracle-Sole, and D. W. Robinson, Commun. Math. Phys. **10**, 311 (1968).
[34] M. Aizenman and B. Nachtergaele, Commun. Math. Phys. **164**, 17 (1994).
[35] D. Ioffe, in *Stochastic Geometry of Classical and Quantum Ising Models*, Springer Lecture Notes in Mathematics (Springer, New York, 2008).
[36] B. B. Beard and U.-J. Wiese, Phys. Rev. Lett. **77**, 5130 (1996).
[37] N. V. Prokof'ev, B. V. Svistunov, and I. S. Tupitsyn, JETP **87**, 310 (1998).
[38] H. Rieger and N. Kawashima, Eur. Phys. J. B **9**, 233 (1999).
[39] H. G. Evertz, Adv. Phys. **52**, 1 (2003).
[40] The weight $w(\boldsymbol{\sigma})$ becomes $\lambda B/N_s$ raised to the number of discontinuities in the spin trajectory and the factors λ/N_s are absorbed in the change in variables from discrete to continuous time.
[41] This can be done with a number of operations of order p. Let us define $\mathcal{Z}_i(\sigma_0,\ldots,\sigma_i|\mathbf{h})=\Sigma_{\sigma_{i+1},\ldots,\sigma_p}\mathcal{Z}(\sigma_0,\ldots,\sigma_p|\mathbf{h})$. First draw σ_0 with probability $\mathcal{Z}_0(\sigma_0|\mathbf{h})/\mathcal{Z}(\mathbf{h})$, then σ_1 according to $\mathcal{Z}_1(\sigma_0,\sigma_1|\mathbf{h})/\mathcal{Z}_0(\sigma_0|\mathbf{h})$, and so on and so forth.
[42] S. Janson, T. Luczak, and A. Rucinski, *Random Graphs* (Wiley, New York, 2000).
[43] This is the graph theoretic distance between two vertices i and j, defined as the length of a shortest path of adjacent vertices joining i and j along the graph.
[44] F. Kschischang, B. J. Frey, and H.-A. Loeliger, IEEE Trans. Inf. Theory **47**, 498 (2001).
[45] J. S. Yedidia, W. T. Freeman, and Y. Weiss, Adv. Neural Inf. Process. Syst. **13**, 689 (2001).
[46] A. Dembo and A. Montanari, arXiv:0804.4726 (unpublished).
[47] F. Alet, P. Dayal, A. Grzesik, A. Honecker, M. Koerner, A. Laeuchli, S. R. Manmana, I. P. McCulloch, F. Michel, R. M. Noack, G. Schmid, U. Schollwoeck, F. Stoeckli, S. Todo, S. Trebst, M. Troyer, P. Werner, S. Wessel, and The ALPS Collaboration, J. Phys. Soc. Jpn. **74**, 30 (2005).
[48] R. H. Swendsen and J.-S. Wang, Phys. Rev. Lett. **57**, 2607 (1986).
[49] O. Redner, J. Machta, and L. F. Chayes, Phys. Rev. E **58**, 2749 (1998).
[50] J. Houdayer, Eur. Phys. J. B **22**, 479 (2001).
[51] T. Jörg, Phys. Rev. B **73**, 224431 (2006).
[52] E. Marinari, G. Parisi, and J. J. Ruiz-Lorenzo, in *Spin Glasses and Random Fields*, edited by A. P. Young (World Scientific, Singapore, 1997).
[53] K. Hukushima and K. Nemoto, J. Phys. Soc. Jpn. **65**, 1604 (1996).
[54] M. Guo, R. N. Bhatt, and D. A. Huse, Phys. Rev. Lett. **72**, 4137 (1994); Phys. Rev. B **54**, 3336 (1996).
[55] H. Rieger and A. P. Young, Phys. Rev. Lett. **72**, 4141 (1994).
[56] H. Rieger, in *Quantum Annealing and Other Optimization Methods*, Lecture Notes in Physics (Springer, New York, 2005).
[57] F. Alet, S. Wessel, and M. Troyer, Phys. Rev. E **71**, 036706 (2005).
[58] R. H. Swendsen and J.-S. Wang, Phys. Rev. Lett. **58**, 86 (1987).
[59] D. P. Landau and K. Binder, *A Guide to Monte Carlo Simulations in Statistical Physics*, 2nd ed. (Cambridge University Press, Cambridge, England, 2005).
[60] *Finite Size Scaling and Numerical Simulation of Statistical Systems*, edited by V. Privman (World Scientific, Singapore, 1990).
[61] E. Brezin, J. Phys. (France) **43**, 15 (1982).
[62] R. Botet and R. Jullien, Phys. Rev. B **28**, 3955 (1983).
[63] J. L. Jones and A. P. Young, Phys. Rev. B **71**, 174438 (2005).
[64] F. Liers, M. Palassini, A. K. Hartmann, and M. Jünger, Phys. Rev. B **68**, 094406 (2003).
[65] T. Jörg, H. G. Katzgraber, and F. Krzakala, Phys. Rev. Lett. **100**, 197202 (2008).
[66] S. Franz, M. Mézard, F. Ricci-Tersenghi, M. Weigt, and R. Zecchina, Europhys. Lett. **55**, 465 (2001).
[67] M. B. Hastings, Phys. Rev. B **76**, 201102(R) (2007).
[68] R. Brout, K. A. Müller, and H. Thoma, Solid State Commun. **4**, 507 (1966).
[69] R. M. Stratt, Phys. Rev. B **33**, 1921 (1986).
[70] L. Chayes, N. Crawford, D. Ioffe, and A. Levit, J. Stat. Phys. **133**, 131 (2008).